

2-9-2010

Incorporation of phase changes in functional magnetic resonance imaging

Sunil Kumar Arja

Follow this and additional works at: https://digitalrepository.unm.edu/ece_etds

Recommended Citation

Arja, Sunil Kumar. "Incorporation of phase changes in functional magnetic resonance imaging." (2010).
https://digitalrepository.unm.edu/ece_etds/21

This Thesis is brought to you for free and open access by the Engineering ETDs at UNM Digital Repository. It has been accepted for inclusion in Electrical and Computer Engineering ETDs by an authorized administrator of UNM Digital Repository. For more information, please contact disc@unm.edu.

Sunil Kumar Arja

Candidate

Electrical and Computer Engineering

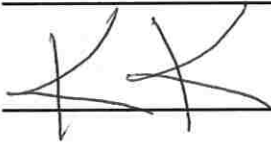
Department

This thesis is approved, and it is acceptable in quality and form for publication:

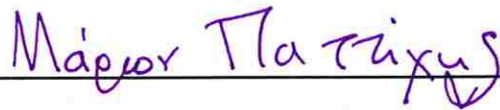
Approved by the Thesis Committee:



, Chairperson



Kent Kiehl, reader



, reader

Incorporation of Phase Changes in Functional Magnetic
Resonance Imaging

By

Sunil Kumar Arja

B.TECH., Electronics and Communications Engineering, Jawaharlal
Nehru Technical University, 2007

THESIS

Submitted in Partial Fulfillment of the
Requirements for the Degree of

Master of Science
Computer Engineering

The University of New Mexico
Albuquerque, New Mexico

December, 2009

© 2009, Sunil Kumar Arja

DEDICATION

This thesis is dedicated to father A. Seshu Babu, mother A Seshu Mani, and a friend for their never-ending support and encouragement. And to my family and friends for their help and support through the process.

ACKNOWLEDGEMENT

I would like to thank Dr. Vince Calhoun, Associate Professor Electrical and Computer Engineering Department, Director, Image Analysis of MR Research, for his guidance, support and encouragement during my Master's program. His valuable suggestions helped me in finishing my thesis with a great success. Through his knack for details, he has always provided me with many insightful observations and valuable comments. I am very grateful for all his advice which has and will be a great value addition to me during my professional career.

I am also grateful to Dr. Kent Kiehl, Associate professor, Psychology Department and Dr Marios Pattichis, Associate Professor Electrical and Computer Engineering Department for being in my committee and guiding me in successfully completing the thesis.

I would like to thank all the members of Medical Image Analysis Lab at The Mind Research Network for their guidance and support. This work is supported by NSF grants 0715022 and 0840895. Finally, I convey many thanks to all my friends for their love and support.

Incorporation of Phase Changes in Functional Magnetic
Resonance Imaging

By

Sunil Kumar Arja

ABSTRACT OF THESIS

Submitted in Partial Fulfillment of the
Requirements for the Degree of

Master of Science
Computer Engineering

The University of New Mexico
Albuquerque, New Mexico

August, 2009

INCORPORATION OF PHASE CHANGES IN FUNCTIONAL MAGNETIC RESONANCE IMAGING

By

Sunil Kumar Arja

B.TECH. in Electronics and Communications Engineering, Jawaharlal Nehru Technical
University, 2007

M.S. in Electrical Engineering, University of New Mexico, 2009

ABSTRACT

Functional magnetic resonance imaging (fMRI) data is acquired as a complex image pair including magnitude and phase information. The vast majority of fMRI experiments do not attempt to take advantage of the time varying phase information. The phase of the MRI signal is related to the local magnetic field changes, suggesting it may contain useful information about the source of hemodynamic activity. Analysis of phase data acquired from different fMRI experiments has shown the presence of activity in response to various stimuli. However, there have been no studies which have examined phase data in a larger group of subjects for multiple types of fMRI tasks, nor have studies examined phase changes due to event-related stimuli. In this thesis, we examine the magnitude and phase changes in group data in a block-design motor tapping task and in an event-related auditory oddball task. We also look at any additional processing steps that might be required for phase. The results for both block-design and event-related tasks indicate the presence of task related information in the phase data with phase only and magnitude only approaches showing signal changes in the expected brain regions. Techniques like temporal smoothing and Gaussian smoothing seem to help improve the results. Although there is more overall activity detected with magnitude data, the phase only analysis also reveals activity in regions expected to be involved in the task, but not significantly activated in the magnitude only analysis, suggesting that the phase might provide some unique

information. In addition, the phase can potentially increase sensitivity within regions also showing magnitude changes. Future work should focus on additional methods for combining the magnitude and phase data

CONTENTS

CHAPTER 1	INTRODUCTION	1
1.1	THESIS ORGANIZATION	2
1.2	CONTRIBUTION OF THIS THESIS	2
CHAPTER 2	FUNCTIONAL MRI/ COMPLEX FMRI	4
2.1	A MEASURE OF BRAIN FUNCTION	4
2.2	BOLD & HRF	5
2.3	ACQUISITION	6
2.4	NOISE	7
2.5	ACTIVATIONS	8
2.6	SUMMARY	8
CHAPTER 3	APPROACHES TO FMRI DATA ANALYSIS	9
3.1	EXPERIMENTAL DESIGN	9
3.1.1	BLOCK DESIGN	10
3.1.2	EVENT-RELATED	11
3.1.3	MIXED DESIGN	13
3.2	FMRI PARADIGM & SUBJECTS	14
3.2.1	MOTOR TAPPING	14
3.2.2	AUDITORY ODDBALL	14
3.3	EXPERIMENTAL PROCEDURE	15
3.4	PRE-PROCESSING	16
3.4.1	SLICE TIMING CORRECTION	16
3.4.2	MOTION CORRECTION	17
3.4.3	COREGISTRATION.....	17
3.4.4	NORMALIZATION	18
3.4.5	SPATIAL SMOOTHING	18
3.5	MODEL BASED APPROACH	20

3.5.1	GENERAL LINEAR MODEL.....	20
3.5.2	CONTRASTS.....	22
3.5.3	THRESHOLDING.....	22
3.6	DATA DRIVEN APPROACH.....	23
3.6.1	INDEPENDENT COMPONENT ANALYSIS	23
3.6.2	CLUSTERING.....	25
3.7	GLM & ICA COMPARISON.....	25
3.8	SUMMARY	26
CHAPTER 4	METHODS FOR ANALYZING AND UNDERSTANDING COMPLEX FMRI	27
4.1	DEALING WITH PHASE	28
4.1.1	MOTION CORRECTION FOR PHASE	28
4.1.2	GAUSSIAN SMOOTHING OF THE TIME COURSES.....	29
4.1.3	COMPLEX DENOISING OF fMRI DATA VIA WAVELET	31
4.1.4	PHASE UNWRAPPING	35
4.1.5	ISSUES WITH THE PHASE DATA	36
4.2	SINGLE SUBJECT ANALYSIS	36
4.3	GROUP ANALYSIS	37
4.4	METHODS	38
4.4.1	WHOLE BRAIN ANALYSIS	38
4.4.1.1	WHOLE BRAIN ANALYSIS FOR MOTOR TAPPING	38
4.4.1.2	WHOLE BRAIN ANALYSIS FOR AUDITORY ODDBALL	38
4.4.1.3	RESULTS AND DISCUSSIONS.....	39
4.4.2	ROI ANALYSIS: TIME LOCKED AVERAGING	41
4.4.2.1	MASKING	42
4.4.2.2	ONSET TIMES	42
4.4.2.3	ROI FOR MOTOR TAPPING	43
4.4.2.4	ROI FOR AUDITORY ODDBALL	43
4.4.2.5	RESULTS AND DISCUSSIONS.....	44
4.4.3	TEMPORAL FILTERING & ICA	47
4.4.3.1	STRINGENT BAND PASS FILTERING	49

4.4.3.2 EFFECTS ON ICA	51
4.4.3.3 RESULTS & IMPROVEMENT	52
4.4.3.4 DISCUSSIONS	57
4.5 SUMMARY	58
CHAPTER 5 CONCLUSIONS AND FUTURE WORKS	64
REFERENCES	66

LIST OF FIGURES:

FIGURE 2.1: HRF TIME COURSE	5
FIGURE 2.2: FMRI ACQUISITION	7
FIGURE 3.1: FMRI BLOCK-DESIGN EXPERIMENT.....	11
FIGURE 3.2: FMRI EVENT-RELATED DESIGN.....	12
FIGURE 3.3: MIXED DESIGN PARADIGM.....	13
FIGURE 3.4: GENERAL LINEAR MODEL.....	21
FIGURE 3.5: INDEPENDENT COMPONENT ANALYSIS.....	24
FIGURE 4.1: GROUP ACTIVATION MAPS FOR NORMAL AND MOTION CORRECTED PHASE	29
FIGURE 4.2: PSD OF THE RESPONSE	30
FIGURE 4.2B: FREQUENCY RESPONSE OF THE GAUSSIAN FILTER	30
FIGURE 4.3: SINGLE SUBJECT ACTIVATION MAPS FOR NORMAL AND GAUSSIAN SMOOTHED PHASE.....	31
FIGURE 4.4: ILLUSTRATION OF THE WAVELET DENOISING ALGORITHM.	33
FIGURE: 4.5 DILATED MASK USED FOR THRESHOLD CALCULATION.....	34
FIGURE 4.6: SINGLE SUBJECT ACTIVATION MAPS FOR NORMAL AND DWT DE- NOISED PHASE.....	34
FIGURE 4.7: WHOLE BRAIN ANALYSIS RESULTS.....	40
FIGURE 4.8: MAGNITUDE AND PHASE FMRI TIME COURSES FOR MT.....	41
FIGURE 4.9: GROUP TIME LOCKED AVERAGING RESULTS FOR MOTOR TAPPING. 45	
FIGURE 4.10: GROUP TIME LOCKED AVERAGING RESULTS FOR AOD.....	46
FIGURE 4.11: POWER SPECTRUM OF THE FMRI TIME COURSE.....	48
FIGURE 4.12: TEMPORAL FILTERING SIMULATION.....	49
FIGURE 4.13: RAW AND BAND-PASS FILTERED TIME COURSES	50
FIGURE 4.14: FREQUENCY RESPONSE OF AN 8TH ORDER BAND-PASS BUTTERWORTH FILTER WITH PASS-BAND FROM 0.05 TO 0.7HZ.....	51
FIGURE 4.15: RAW AND BAND-PASS FILTERED TIME COURSES FOR THE GENERALIZED PARAMETERS.....	52
FIGURE 4.16: EFFECTS FOR TEMPORAL FILTERING ON REAL TIME DATA.....	53
FIGURE 4.17: ICA RESULTS FOR UNFILTERED DATA.....	54
FIGURE 4.18: ICA RESULTS FOR FILTERED DATA	55
FIGURE 4.19: BAR PLOT OF HOW INDIVIDUAL AND GROUP ICA REACTED TO TEMPORAL FILTERING OF MAGNITUDE.....	56

FIGURE 4.20: BAR PLOT OF HOW INDIVIDUAL AND GROUP ICA REACTED TO TEMPORAL FILTERING OF PHASE	56
---	----

LIST OF TABLES:

TABLE 1: TALAIRACH TABLE FOR MOTOR TAPPING	59
TABLE 2: TALAIRACH TABLE FOR AUDITORY ODDBALL	60
TABLE 3: TALAIRACH TABLE FOR RGB MAPS OF MOTOR TAPPING	61
TABLE 4: TALAIRACH TABLE FOR RGB MAPS OF AUDITORY ODDBALL	62

CHAPTER 1

INTRODUCTION

Human brain is a barely explored new world. The ability to image and understand the functioning of the human brain opens a window of new opportunities to advance our understanding of brain organization. Functional Magnetic Resonance Imaging (fMRI) helps us achieve this. FMRI is a neuro-imaging technique that uses MRI imaging to investigate changes in the brain function over time. It can reveal the parts of the brain that were activated by behavioral task with a spatial resolution of around 2 millimeters, which is better than many other neuroscience techniques. The Magnetic properties of hemoglobin change depending on whether it is oxygenated or deoxygenated. Oxyhemoglobin (HbO₂) is diamagnetic but when it loses the oxygen it turns into Deoxyhemoglobin (Hb) which is paramagnetic (Pauling and Coryell 1936). Thus hemoglobin present in blood can be used as the contrast agent and this type of contrast is called blood oxygenation dependent contrast (BOLD) contrast. This BOLD contrast helps in the detection of oxygenation and thus the brain activation.

Functional magnetic resonance imaging (fMRI) data is acquired as a complex image pair (or multiple pairs), with both the magnitude and the phase of signal. This complex-valued fMRI signal has been shown to contain physiologic information. The response in the magnitude image is typically obtained by correlating the fMRI data with an assumed reference signal (Bandettini, Jesmanowicz et al. 1993). In spite of the presence of useful information in phase, it is usually completely discarded. Previous studies have reported task-related phase changes (Hoogenraad, Reichenbach et al. 1998; Hoogenraad, Pouwels et al. 2001; Menon 2002; Rowe 2005). Several approaches for modeling the phase models have been proposed (Rowe and Logan 2004; Rowe

2005; Rowe and Logan 2005). Processing complex-valued fMRI data using independent component analysis was also proposed in (Calhoun, Adali et al. 2002). Previous work has focused on filtering voxels with large phase changes (Menon 2002; Tomasi and Caparelli 2007; Zhao, Jin et al. 2007) based upon models, which shows that phase changes arise only from large non-randomly-oriented blood vessels. More recent studies from our group and others provide evidence that the randomly oriented microvasculature can also produce a non-zero BOLD-related phase change (Zhao, Jin et al. 2007; Feng, Caprihan et al. 2009) suggesting that the phase information contains useful physiologic information.

1.1 THESIS ORGANIZATION

This thesis is organized in the following manner. Chapter 2 gives an overview of Functional MRI/ Complex fMRI, properties of the signals, physics involved, activations etc. Chapter 3 discusses the approaches to fMRI data analysis, pre-processing the data, model based approach, data driven approach and concludes with a summary of the pros and cons of each approach. Chapter 4 discusses the problems encountered while dealing with phase, the methods we used for analyzing and understanding Complex fMRI and concludes with results. In Chapter 5 we discuss the summary of our work, conclusions and future work need.

1.2 CONTRIBUTION OF THIS THESIS

Previous research has reported phase changes in block design tasks (Miller, Hargreaves et al. 1-5 Sept. 2004; Deshmukh, Shivhare et al. 20-22 Dec. 2004; Weaver 1999; Calhoun, Adali et al. 2002; Laird, Rogers et al. 2002; Rowe 2005; Lee, Shahram et al. 2007; Zhao, Jin et al. 2007; Natalia Petridou, Andreas Schäfer et al. 2009) in single subjects, but to our knowledge no study has yet evaluated phase changes during an event related design task, nor are we aware of any

studies of phase changes evaluated at a group level. Our goal is to evaluate task-related phase changes compared to the task-related magnitude changes in both block design tasks and event related tasks. This thesis particularly focuses on the following objectives, a) evaluating the degree to which the voxels are activated in both phase and magnitude, b) evaluating the degree to which the voxels showed only phase change or only magnitude change, c) evaluating whether phase changes can be detected in both block and event-related designs and d) evaluate the effects of additional processing strategies that might be required for phase. In addition to addressing the four main objectives, the degree to which the active voxels occur in regions expected to be activated by the task are also evaluated.

In our thesis we analyze the phase changes across two different fMRI experimental paradigms (motor tapping and auditory oddball) via both region of interest analysis and whole brain analysis. The phase information is analyzed using a standard group analysis for both paradigms. We then compare the phase changes observed with those of the magnitude to observe the consistency of the phase activation with that of magnitude. The phase data and the magnitude data are separately analyzed and the convergence of the results is then evaluated. The identification of regions which were 1) detected for only magnitude data, 2) detected for only phase data, or 3) detected for both magnitude and phase data were of particular interest. It is expected that by incorporating the phase information collected as a part of standard BOLD fMRI experiment the analysis of whole brain BOLD fMRI data can be potentially improved.

CHAPTER 2

FUNCTIONAL MRI/ COMPLEX FMRI

Functional magnetic resonance imaging (fMRI) is the most popular tool used to measure the brain function. It helps understand the parts of the brain that are being used to do a given cognitive task. Though the temporal resolution is relatively low, the spatial resolution of fMRI is high making it one of the superior methods in cognitive neuroscience. In this chapter, we start our discussion with an introduction to the fMRI technique as an important way to measure of brain function. We then discuss the acquisition of the fMRI signal. We discuss the different types of effects involved in fMRI data. We discuss the properties of signals and types of noises, signal to noise ratio and the artifacts involved in the fMRI data. The statistical properties of the data are also presented.

2.1 A MEASURE OF BRAIN FUNCTION

Magnetic Resonance Imaging, or MRI, typically measures the response of hydrogen molecules to any magnetic changes while in a magnetic field. The same MRI principal and equipment can be used to look at the functional changes in the brain (in response to a cognitive task), it is referred to as functional magnetic resonance imaging (fMRI). BOLD (blood oxygenation level-dependent contrast) technique is the commonly used technique in fMRI. BOLD technique is based on the fact that, magnetic properties of oxygenated (diamagnetic) and deoxygenated (paramagnetic) blood are different. These differences in magnetic susceptibility (from diamagnetic to paramagnetic) play a very prominent role in measuring the brain function. It is well known that different cognitive tasks activate different regions in the brain. When brain

neurons are active, they use the oxygen present in the blood, this results in a change in blood flow and oxygenation, which causes a change in the signal. By studying the locations of these signal changes for a given task, the regions that are being used to do a given cognitive task can be studied.

2.2 BOLD & HRF

BOLD fMRI measures the inhomogeneity in the magnetic field as a result of the changes in the level of oxygen present in the blood (blood oxygenation) (Ogawa, Lee et al. 1990; Detre and Wang 2002; Heeger and Ress 2002). When the hemoglobin protein contained within the red blood cells loses the oxygen molecule (it becomes deoxyhemoglobin), its magnetic properties change, this will cause an inhomogeneity in the magnetic field surrounding it. The more deoxyhemoglobin in blood, the more the inhomogeneity will be, hence the more the decrease in the fMRI signal. The temporary increase in the neuronal activity will generate a BOLD fMRI signal, its function against time is known as the hemodynamic response function (HRF) shown in the Figure 2.1.

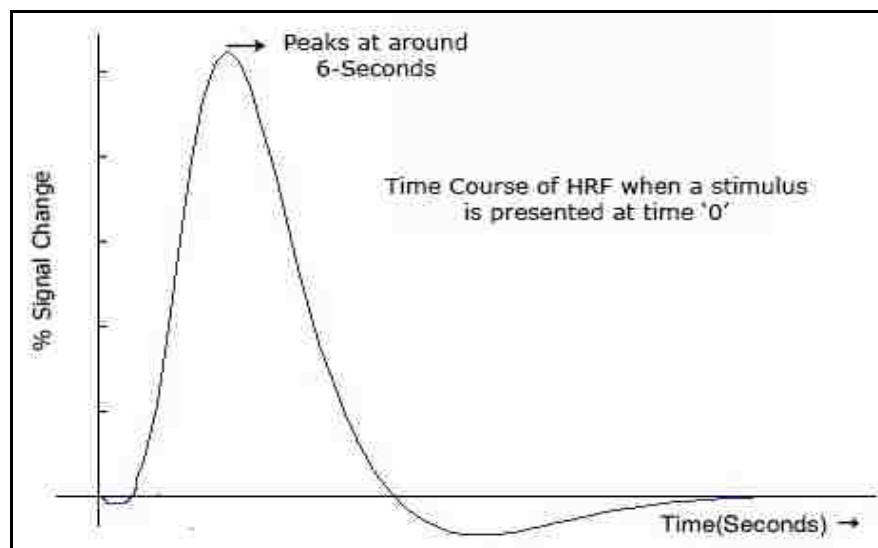


Figure 2.1: HRF time course

When the neuronal activity begins, the fMRI BOLD signal initially decreases a little as the active neurons use the oxygen causing a drop in the oxyhemoglobin level (this is very small and is not always observed). After this tiny dip, due to the over supply of oxygen, there is a very large increase in the signal. The signal reaches its peak at around 6 seconds. The over supply of oxygen will cause a large decrease in the level of deoxyhemoglobin, thereby generating a large fMRI BOLD signal. As the level of deoxyhemoglobin slowly returns to the normal level and the signal decays, after an initial underfoot the signal returns to the baseline approximately after 24 seconds. The function of the BOLD fMRI signal against time is called the BOLD response.

2.3 ACQUISITION

The MRI signal is acquired using two orthogonal detectors as shown in the Figure-2.2 (Hoult, Chen et al. 1984). The output is in complex form, one of the detector's output is taken as the real part and the other detector's output as the imaginary part. The data is in frequency space, so inverse fourier transform is performed to get the data into complex image space. Once the data is in the complex image space, the magnitude and phase of the data is calculated. The functional magnetic resonance imaging (fMRI) data is stored as a complex image pair including magnitude and phase information.

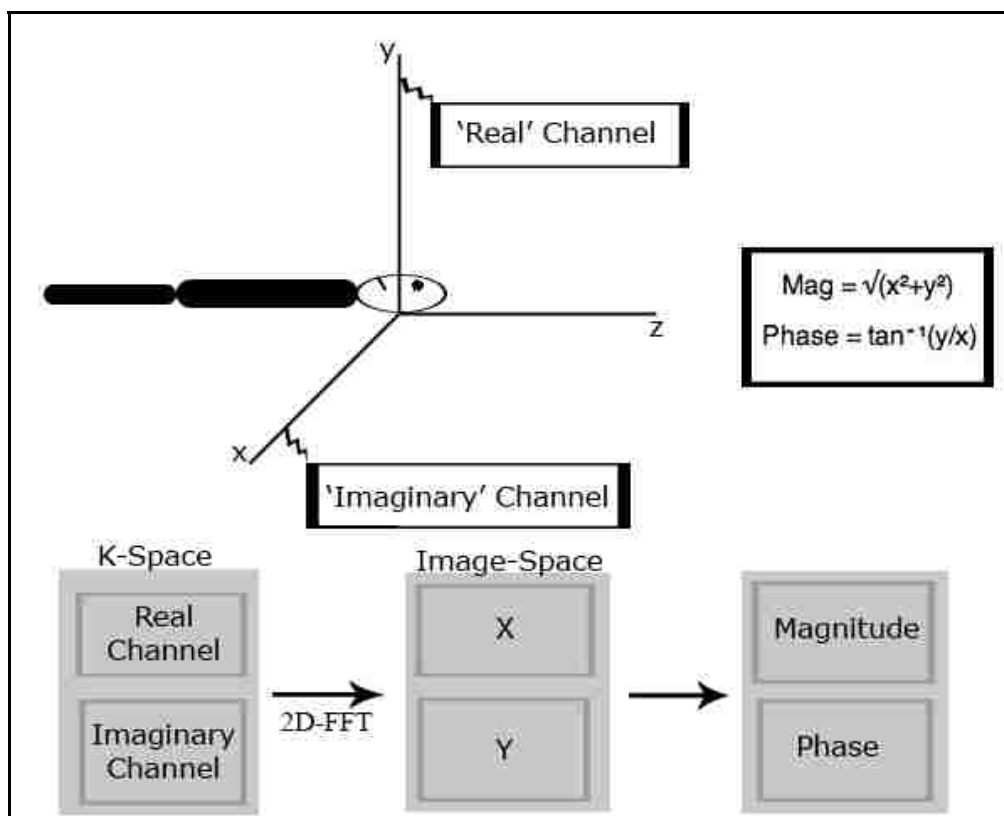


Figure 2.2: fMRI Acquisition

In spite of the low contrast to noise ratio of the fMRI data, most studies analyse only the magnitude images. The basic approach is to correlate the data magnitude time series with a predetermined reference signal. The most popular is the general linear modeling approach, it utilizes the hemodynamic response to measure the activation. But none of these approaches look at the phase information.

2.4 NOISE

Various types of noise affect the fMRI data. The different noises include thermal noise, which is responsible for variation in background eddy currents; scanner heating, power fluctuations typically caused by scanner problems. Then there is noise due to head motion effects, physiological changes like the heart rate and breathing, differences across brain regions

like functional differences and large vessel effects and last of all the artifact-induced problems. The thermal noise will result in white noise with constant noise in the data. The presence of these noises can cause negative and positive false activation and obscure true activated pixels. The independent component analysis which is discussed in Chapter-3 will separate noise as a different component in the data.

2.5 ACTIVATIONS

There are many techniques available for statistically analyzing fMRI data. The aim of any such technique is to generate a map of the human brain identifying the regions that show significant signal change in response to the task. Each voxel is assigned a value depending on the likelihood between the signal change at that voxel and the model. The maps so generated are called activation maps or statistical parametric map. The data driven techniques like ICA make no prior assumptions about the model response. The activation maps are generated based on components; this is discussed later in Chapter-3.

2.6 SUMMARY

Functional magnetic resonance imaging (fMRI) is a very useful non-invasive tool to study the brain function. In spite of its limitations, it is one of the superior methods available in cognitive neuroscience. We have provided a brief introduction to the fMRI techniques, measurable brain functions and the acquisition of the fMRI signal. We also discussed the properties of signals and types of noises involved in the fMRI data and activations. In the next chapter we discuss the approaches available for fMRI data analysis.

CHAPTER 3

APPROACHES TO FMRI DATA ANALYSIS

In this chapter an overview of common fMRI analysis methods is given. We start the discussion with the key concepts of experimental design then continuing to the discussion of the fMRI paradigm & subjects, procedures of preprocessing and concluding with a description of the approaches for studying fMRI data like the general linear model and the independent component analysis. Almost all the fMRI studies use either block design or event related design, we discuss the advantages and disadvantages of each design and consider advanced design types that combine both event related design and block design. The main goal in doing preprocessing is to reduce the variability in the data that is unrelated to the experimental task. The steps include slice time correction, correction for head motion, and co-registration and normalization of the data to reduce the variability in the size, shape and orientation of the brain in the subject group. After the pre-processing steps, statistical analysis is carried out to determine which voxels are activated by the stimulation. There are different approaches available for the statistical analysis, methods that are model based and methods that are data driven which are discussed in detail in this chapter.

3.1 EXPERIMENTAL DESIGN

Experimental design mainly deals with the organization of experiment to effectively test the research hypothesis. By controlling the timing and quality of presented stimuli we can study its influence on the resulting brain processes. What can we effectively control? Experimental comparisons (what is to be measured?), stimulus properties (what is presented?), stimulus timing (when is it presented?), subject instructions (what do subjects do with it?). Our main goal is to

increase the Detection (What is active?) and Estimation (How does its activity change over time?) by tuning the way the stimuli are presented. An optimal experimental design would maximize both detection & estimation. Maximizing variance in stimulus timing (increases estimation) and variance in measured signal (increases detection) helps achieve this. Before we go into the discussion of common design procedures, let us look at a few basic elements and principles of experimental design.

The fundamental element of an experiment is the “variable”. There are two types of variables, Independent variables and Dependent variables. Independent variables are the variables that we can control on the experiment; these are expected to cause changes in the dependent variables. The choice of these independent variables depends on the hypothesis to be tested. Dependent variables are the ones measured in the experiment to evaluate the effects of the independent variables. They give evidence for or against the hypothesis; so having multiple dependent variables helps. Two design procedures most commonly used are Block design and Event-Related design, which is discussed below.

3.1.1 BLOCK DESIGN

Block design is the separation of the experimental conditions into distant blocks. Each block is presented for an extended period of time, and the effect of the independent variable on the dependent variable is studied. This is the simplest and most powerful way to design the experiment and is also known as the boxcar. This is still the most commonly used experimental design in neuroimaging. If we consider a simple block design experiment as shown in the Figure 3.1; two conditions are alternated in blocks.

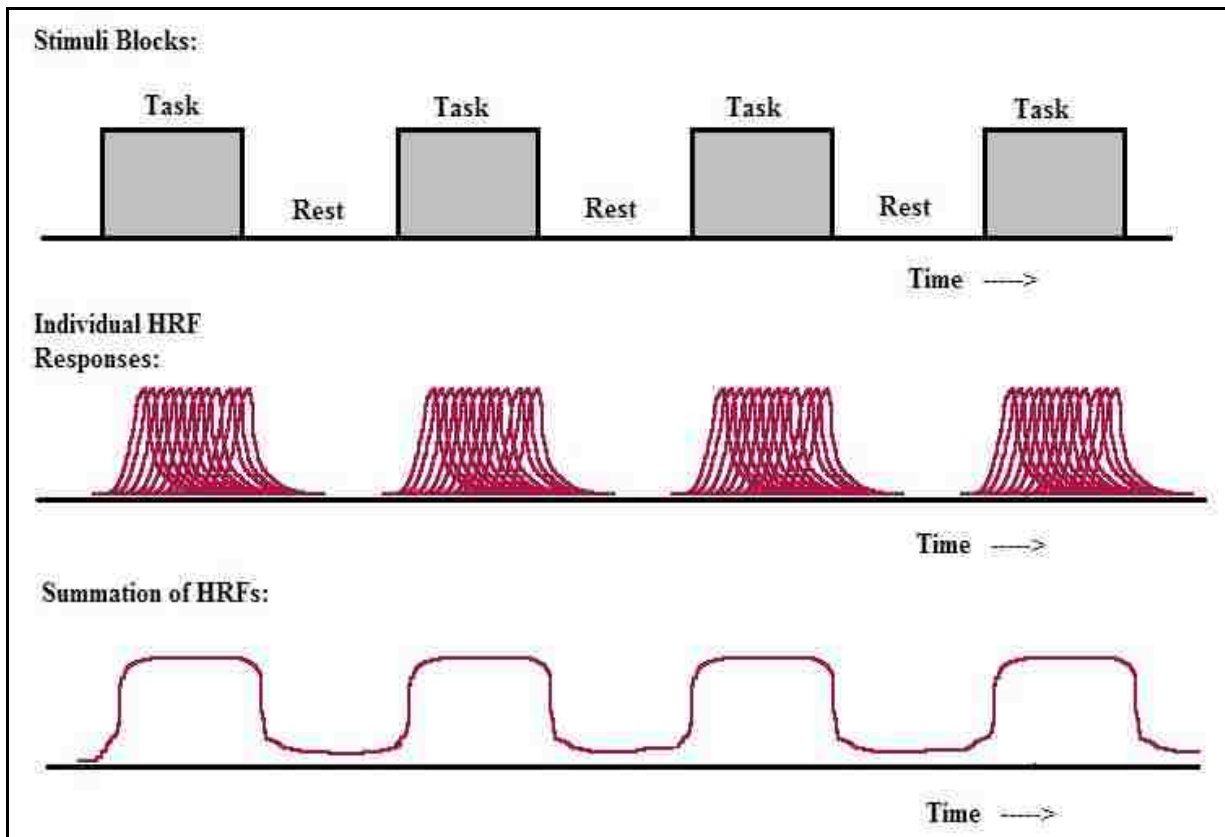


Figure 3.1: fMRI Block-Design Experiment

Within each block only one condition is presented and a certain number of fMRI scans are collected. By altering the blocks within the cognitive process, the fMRI signal is studied and it represents the cognitive process of interest. The main advantage of block design is the additive nature of the fMRI response. As shown in the Figure-3.1, the amplitude of the HRF increases when multiple stimuli are presented in rapid succession. When each block is alternated with a rest condition in which the HRF has enough time to return to baseline, a maximum amount of variability is introduced in the signal.

3.1.2 EVENT-RELATED

Event related design is the second commonly used experimental design. An event (also know as trail) is a single instance of experimental manipulation. So event related design deals

with the presentation of discrete, short duration events whose order is randomized. In event related design it is assumed that the neural activity of interest will occur for discrete and short intervals when an event occurs. Each event is separated from its previous event with an inter-stimulus interval (ISI) that ranges between 2-10 seconds depending on the experiment.

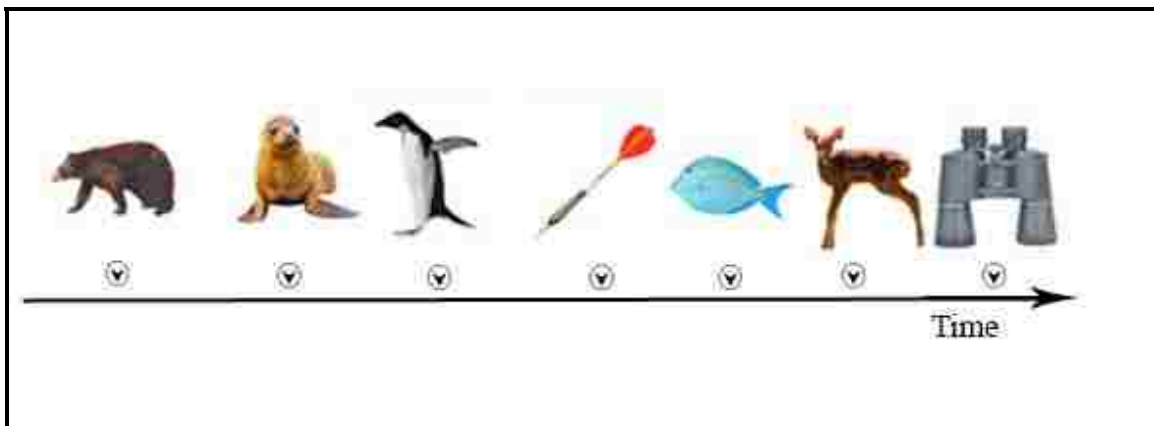


Figure 3.2: fMRI Event-Related Design

Unlike block design, the events are presented in a randomized order and approximate linearity of the BOLD response in response to successive presentations of stimuli, allows stimuli to be presented in relative quick succession in an event-related fMRI design. The statistical power of event related designs is inherently low, because the signal change in the BOLD fMRI signal following a single stimulus presentation is small. Despite the inherent low power of event related designs, there are many advantages in using event related design. The main advantage is that it allows for randomization of trials, so the potential confounds like habituation, anticipation and strategy effects are minimized. This helps us draw solid conclusions and make meaningful inferences. Another advantage of event related designs over block designs is that they allow for removal of certain trials. For example, if a subject has to make a response to a stimulus, it can be

desirable to be able to remove the HRF following stimuli associated with the wrong responses post hoc.

3.1.3 MIXED DESIGN

The third type of fMRI design is the mixed design, it combines the basic elements of both event related design and block design. The stimulus is presented in discrete regular blocks with each block containing multiple types of events as shown in the Figure-3.4.

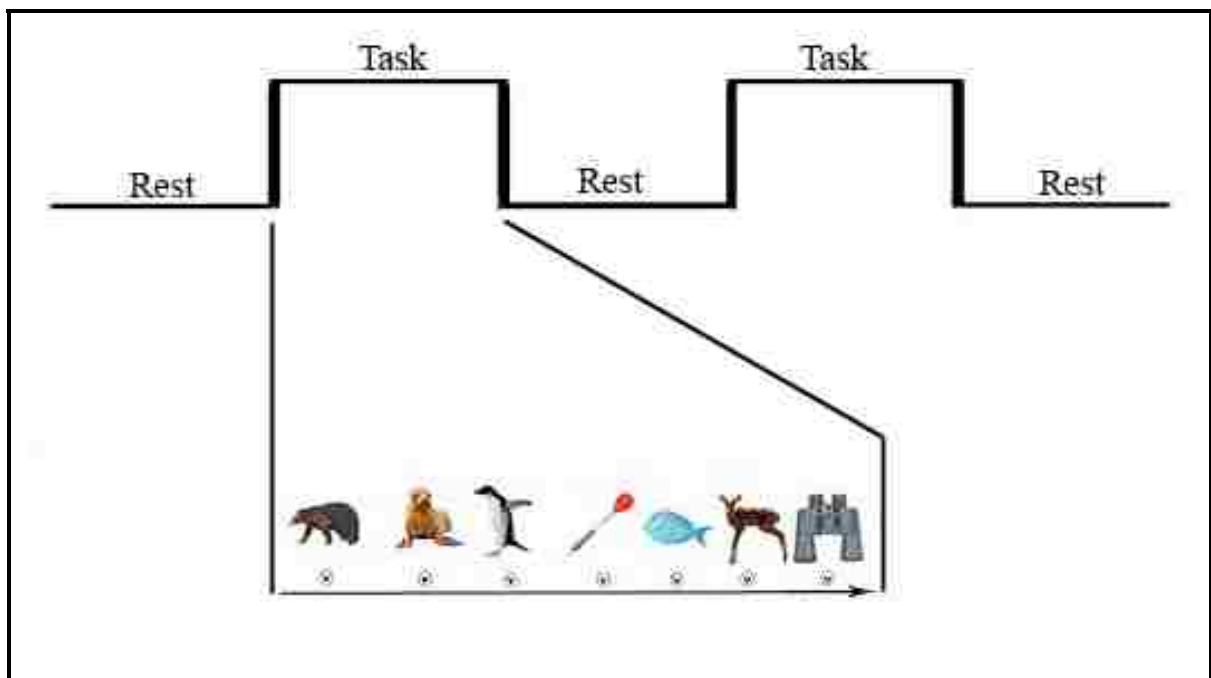


Figure 3.3: Mixed Design Paradigm

Each task block may last for 20 to 30 seconds or more, and are associated with sustained changes in task strategy, attention, or other cognitive processes. The main advantage of mixed design is that it gives the best combination of detection and estimation. It can dissociate transient and sustained components in the brain activity. The only disadvantage is that it relies on assumptions of linearity and is a complicated analysis.

3.2 FMRI PARADIGM & SUBJECTS

3.2.1 MOTOR TAPPING

The first paradigm is a motor tapping (MT) paradigm; a block design with periods of 30 s OFF and 30 s ON. The subjects tapped their fingers during the ON period and rest during the OFF cycle. There were five and a half cycles, starting with OFF and ending with the OFF period. 165 whole head fMRI images were collected for each subject. The total experiment time was 5.5 minutes. The data was collected from 20 healthy subjects participated in the motor tapping experiment, 17 subjects were right handed, 3 subjects were left handed and in the age group between (18-62) years, with 12 male subjects and 8 female subjects.

3.2.2 AUDITORY ODDBALL

The second paradigm was an event-related design, a three-stimulus auditory oddball (AOD), two runs of 244 auditory stimuli consisting of standard, target, and novel stimuli were presented to the subject. The standard stimulus was a 1000 Hz tone, the target stimulus was a 1500 Hz tone, and the novel stimuli consisted of non-repeating random digital noises. The target and novel stimuli each was presented at a probability of 0.10, and the standard stimuli with a probability of 0.80. The stimulus duration was 200 ms with a 2000 ms stimulus onset asynchrony (SOA). Both the target and novel stimuli were always followed by at least 3 standard stimuli. Steps were taken to make sure that all participants could hear the stimuli and discriminate them from the background scanner noise. Subjects were instructed to respond to the target tone with their right index finger and not to respond to the standard tones or the novel stimuli.

For the auditory oddball experiment, the data was collected from 34 healthy, right-handed, male volunteers in the age group from 18-61. IRB-approved informed consent at the

University Of New Mexico was obtained from all the participants. Each participant was presented with a practice block of 10 trials prior to the actual scan to ensure understanding of the instructions. Omission errors included any missed target tones or any response with a latency of greater than the reaction time from target stimulus.

3.3 EXPERIMENTAL PROCEDURE

All MT imaging was performed on a 3T Siemens TIM system with a 12-channel radio frequency (RF) coil. The fMRI experiment used a standard Siemens gradient-echo EPI sequence modified so that it stored real and imaginary data separately. The following parameters were used: Field-of-View (FOV) = 24cm, Slice Thickness = 3.5 mm, Slice Gap = 1 mm, Number of slices = 32, Matrix size = 64×64, TE = 29ms, TR = 2s, flip angle 70 deg. We collected 15 whole head fMRI images during each ‘ON’ or ‘OFF’ period. Data collection was prefaced by a 12 s rest period that was collected to allow for T1 effects to stabilize. All AOD imaging was performed on a 1.5T Siemens Avanto TIM system with a 12-channel RF coil. Conventional spin-echo T1 weighted sagittal localizers were acquired for use in prescribing the functional image volumes. Functional image volumes were collected with a gradient-echo sequence, modified so that it stored real and imaginary data separately, with the following parameters: FOV = 24 cm, slice thickness = 4.0 mm, Slice Gap = 1 mm, Number of slices = 27, Matrix size = 64×64, TE= 39ms, TR= 2s, flip angle 75 deg, 3.8 x 3.8 mm in-plane resolution. The participant’s head was firmly secured using a custom head holder. The two stimulus runs consisted of 189 time points, prefaced by a 12 s rest period that was collected to allow for T1 effects to stabilize. These initial four images were not included in any subsequent analyses.

3.4 PRE-PROCESSING

In a typical fMRI experiment the human brain is scanned once in every 2 to 4 seconds, resulting in several brain volumes per experiment for each subject. The data is sensitive to many factors like noise, motion, variability in size and shape across the subjects, so correcting for non-task-related variability in experimental data is necessary. Preprocessing the data plays an important role in the data analysis. It's usually done without consideration of experimental design; thus, pre-analysis (occasionally called post-processing, in reference to being after acquisition) attempts to remove, rather than model, data variability. To achieve this, a number of steps are performed to temporally (slice timing correction) and spatially (motion correction, coregistration, normalization, spatial smoothing etc.) adjust the fMRI data. We now discuss each of these steps and their consequences for data interpretation.

3.4.1 SLICE TIMING CORRECTION

The brain volume consists of a number of slices and each slice consists of a number of voxels. Typically several 2D slices make up a 3D volume, and not all the 2D slices are collected at the exact same time. But in the statistical analysis it is assumed that the entire volume is collected at one point in time, every voxel measured at the same time instant. Since not all the 2D slices are acquired at the same instant, it might seem as though the same change in the BOLD fMRI response starts at an earlier time for slices that are acquired later in time than for slices that are acquired earlier in time. So to correct these differences in the slice acquisition timing, we do slice timing correction (Smith 2001). It corrects for differences in acquisition time within a TR. This is especially important for long TRs (where expected HDR amplitude may vary significantly). First, a decision must be made as to which slice is going to be the reference slice.

Usually, either the first slice or the middle slice of the image of the brain is taken as the reference slice. Once the reference slice is selected, all the other slices in the volume of the brain are shifted in time using an interpolation method.

3.4.2 MOTION CORRECTION

A typical fMRI experiment would last anywhere from 3-10mins, though subjects are instructed not to move inside the scanner, some head movement is unavoidable. This results in the same voxel representing different locations in the brain throughout time (Brammer 2001; Ashburner and Friston 2003). In the statistical analysis, however, we assume that a given voxel represents the same location in the brain throughout time. But when a given voxel moves over time, from a location of the brain with a low fMRI signal to a location of the brain with a higher fMRI signal, it appears as though there was an increase in the fMRI signal for that voxel over time while in reality there was no increase in the fMRI signal. Each subject is spatially adjusted to remove the effects of motion. The first scan in the time series is taken as the reference and all the other volumes are repositioned to match the position of the reference volume. A least mean square difference algorithm is used to do the job.

3.4.3. COREGISTRATION

The functional data is typically low resolution and has low anatomical contrast. Because of this limitation, it is often mapped on to a high resolution and high contrast structural image. The coregistration algorithms do this mapping. There are a number of reasons to perform a coregistration. It helps in accurately determining the location of a statistical increase in the fMRI signal for a subject; it is helpful to be able to overlay the statistical map on a high resolution

anatomical scan of that same subject. It also helps with spatial normalization. The high resolution anatomical scan is more detailed than the fMRI scans, so normalization of the high resolution anatomical scan to a standard brain often leads to better results than matching the fMRI scans to the standard brain. There are a few disadvantages associated with coregistration, it may severely distort functional data and if not done properly, may reduce correspondence between functional and anatomical images.

3.4.4 NORMALIZATION

In any fMRI experiment data is collected from several subjects. However, not all brains come in the same size and shape, and are not oriented alike. So a given voxel in the brain of a subject might not represent the same anatomical location in another subject. This makes comparisons over and between different subjects impossible. To overcome this problem, it is necessary that the size, shape and orientation of the brains of individual subjects be changed to match a standard brain template. This matching of individual brains to a standard template is known as spatial normalization. The main advantage of normalization is that it allows generalization of results to larger population; improves comparison with other studies and helps reporting results. But normalization has its own disadvantages, it reduces spatial resolution, is time consuming, potentially problematic and bad normalization is much worse than not normalizing.

3.4.5 SPATIAL SMOOTHING

It might seem counter productive to spatially blur the images, but there are many good reasons to do so. In fMRI data, the signal of interest produced by changes in blood flow is

mainly present in the low spatial frequency bands and the noise is usually present in higher spatial frequency bands. Hence smoothing the dataset helps increase the signal to noise ratio in the fMRI signal by removing the high spatial frequencies. Smoothing is generally performed by convolving the 3D volume with 3D Gaussian kernel. The Full Width Half Maximum (FWHM) is used to define the shape of the smoothing curve with size typically two or three times the voxel size. It removes small frequency differences, and makes comparisons across subjects easier. Smoothing also helps satisfy the requirements for applying Gaussian Field Theory to correct for multiple comparisons by making the data more normally distributed (Smith 2001). But smoothing has a few disadvantages too, it reduces the spatial resolution and is challenging if size/shape of signal is not known.

In our analysis we used the magnitude and phase images written out as 4D nifti files by a custom reconstruction program on the scanner. Preprocessing of the data was done using the SPM5 software package (<http://www.fil.ion.ucl.ac.uk/spm/software/spm5/>). Magnitude data was co-registered using INRIAlign (Freire and Mangin 2001; Freire, Roche et al. 2002) to compensate for movement in the fMRI time series images. Images were then spatially normalized into the standard Montreal Neurological Institute space. Following spatial normalization, the data (originally acquired at $3.75 \times 3.75 \times 4.5 \text{ mm}^3$) were slightly sub-sampled to $3 \times 3 \times 3 \text{ mm}^3$, resulting in $53 \times 63 \times 46$ voxels. Motion correction and spatial normalization parameters were computed from the magnitude data and then applied to the phase data. The magnitude and phase data were both spatially smoothed with a $10 \times 10 \times 10 \text{ mm}^3$ full width at half-maximum Gaussian kernel; phase and magnitude data were masked to exclude non-brain voxels. Activation maps were computed for both magnitude and phase data using the multiple regression frame work within SPM5 in which regressors are created from the stimulus onset times and

convolved with a standard hemodynamic response function. A contrast was created for each individual subject for finger tapping versus rest. To compute the group maps a second level analysis was performed using the activation maps from each individual subjects and entering them into a one-sample t-test.

3.5 MODEL BASED APPROACH

After the pre-processing steps, statistical analysis is carried out to determine which voxels are activated by the stimulation. This can be simple correlation analysis or more advanced modeling of the expected hemodynamic response to the stimulation. Various possible statistical corrections can be included, such as correction for smoothness of the measured time series at each voxel. The main output from this step is a statistical map, which indicates those points in the image where the brain has activated in response to the stimulus. Let's discuss the aspects of the model-based approach in more detail.

3.5.1 GENERAL LINEAR MODEL

A linear model can be represented mathematically as:

$$y = a_0 + a_1x_1 + a_2x_2 + a_3x_3 + \dots + a_nx_n + e$$

The observed data is the combination of several model factors (x_i) and an error (e). The contribution of each factor is determined by its weight (a_i). The term a_0 is the contribution of the factors that are constant throughout the experiment. The fMRI data can be modeled as a linear model as shown above. The magnitude images of the experiment are the observed data, and the model components are the hypothesized data. So for a given set of observed data and model components, we calculate the combination of the model weights that minimize the error

term. The general linear model (GLM) for the fMRI data in matrix form can be represented as shown below.

$$X = G \times \beta + \varepsilon$$

GLM's main goal is to find the set of experimental parameters (β) for the design matrix (G) that give the least error (ε) or in other words perfectly fit the data (X).

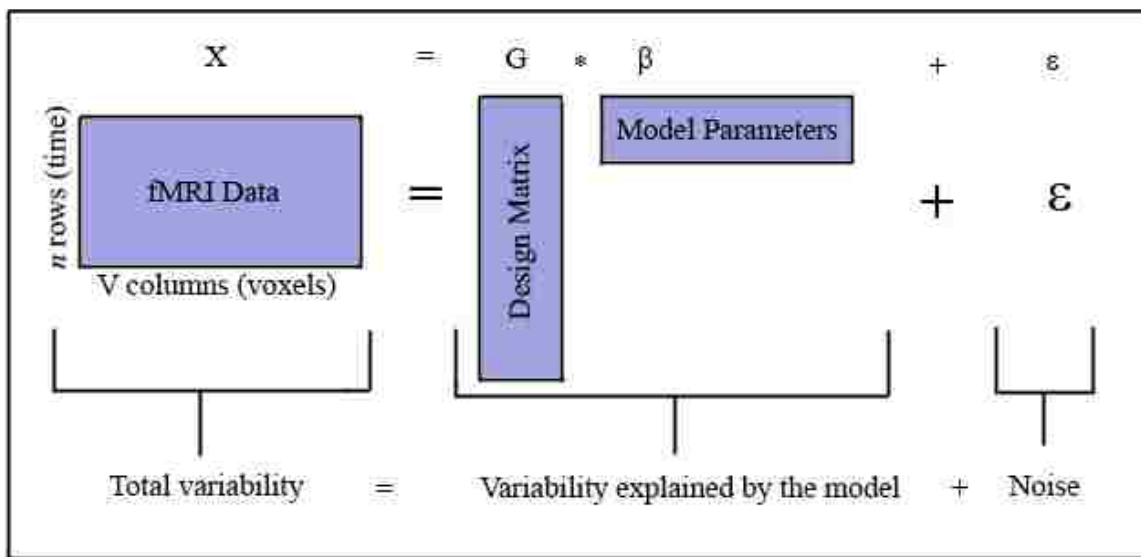


Figure 3.4: General Linear Model

The block diagram of the matrix form of GLM is shown in Figure-3.3. All the voxels in the 3D brain structure are restructured into a 1D array for the ease of computation. The data is modeled as a two dimensional matrix of number of time points (n) (rows) by voxels (V) (columns). GLM does not consider the spatial location of the voxels. The M - model factors and their associated time points form another two-dimensional matrix, this is called the design matrix. The M by N parameter matrix gives the amplitude of the model factors at the given

voxel. The residual variability in the data that remains unaccounted for will be represented in the error matrix.

3.5.2 CONTRASTS

The general linear model gives us the amplitude of the model factors, or in other words the regressors. A given fMRI experiment can have multiple conditions (multiple regressors or model factors) like presenting different kinds of tones as in the auditory oddball (AOD) paradigm. It might often be the case where we might be interested in the difference between two conditions (like between novels and standards in AOD). This can be done by the linear combination of the parameters. This linear combination of parameters is called contrast. To test the difference between two conditions, we can define a matrix C whose columns define linear combinations of the predictors. Lets assume we have three conditions, if we define the contrast matrix C as $[1 \ -1 \ 0]$, it gives us the difference between the first two conditions. This contrast matrix is applied to the beta weights to estimate the effect of interest.

3.5.3 THRESHOLDING

The GLM analysis will generate the statistical maps; in order to decide which parts of the human brain were active we must threshold the data. Thresholding helps us decide which regions are active at a given level of significance. The simplest way to do this is by selecting a significance threshold (p) and applying it to all the voxels in the statistical map. But there is a problem associated with this. If we test the significance of 10,000 voxels at a significance level of $p < 0.01$, it is expected that 100 voxels are activated by chance. This problem is referred to as multiple-comparisons problem, meaning that it is not valid to accept all activation reported;

correction for number of false positives is necessary. The common method used is Bonferroni correction, this corrects for the number of comparisons being made by dividing the significance level at each voxel by the number of voxels. Gaussian random field theory is also used as a possible way to threshold the data.

3.6 DATA DRIVEN APPROACH

The model-based approaches require an accurate estimate of the fMRI signal measured while performing the task. When we look at the voxel's time course to measure the activation, we calculate how well the time course fits the predefined model. The potential problem associated with this is that the model may not be valid, or the subject may not be doing the task correctly or not doing it at all. So a different way of looking at the activation is through data driven analysis. In a data driven approach, we analyze the structure of the data with an expectation that the task related activations would appear. The popular data driven approaches are the independent component analysis (ICA) and clustering. Lets discuss them in detail.

3.6.1 INDEPENDENT COMPONENT ANALYSIS

FMRI signal is a linear combination of signals, with a little knowledge about the source of the mixing process. This is referred to as blind source separation. ICA is the most commonly used data driven approach to solve this problem. The data is an instantaneous linear mixture of generative source signals that can be mathematically represented as

$$X=AS$$

X – Observed Data

A – Mixing Matrix

S – Source Signals

ICA assumes that the source signals are statistically independent from each other. So the goal is to find the source signals and the mixing matrix, which when combined, will give an accurate estimate of the observed data. In fMRI analysis, it is assumed that the data can be segregated in groups of voxels that vary together over time and are maximally independent from the activity in other groups. The time course associated with each group of voxels is called a component. A given voxel can be a part of multiple components. ICA is completely blind to the experimental task or hypotheses. The main challenge is to determine how many components are to be isolated from the data set. The more the number of components the more difficult it is to interpret the data. The basic principle of ICA is illustrated in the Figure-3.4. If we consider a simple model with two sources as shown in the figure, the scanned data will be the mixture of the sources along with their mixing functions. The goal of ICA is to separate these sources so that they are maximally statistically independent.

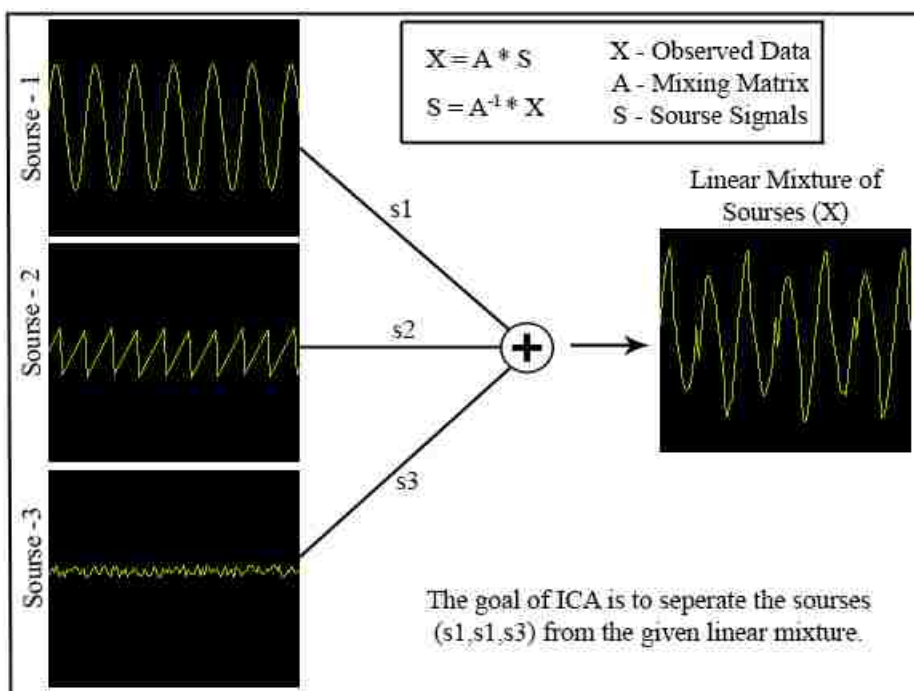


Figure 3.5: Independent Component Analysis

3.6.2 CLUSTERING

Clustering fMRI time series has emerged in recent years as a possible alternative to general linear modeling approach. It is a data-driven approach that looks for clusters of voxels with similar time courses. A mathematical estimate (clustering metric) of the similarity between the time courses is created and the voxels are segregated into distinct clusters based on the metric. So a good solution to any clustering problem depends on the choice of the clustering metric and the dependability of the clustering algorithm. The main questions in any clustering analysis are, how many clusters are needed? And which clustering algorithm should be used? Choosing the right number of clusters plays a very important in clustering. If the number of clusters is small, the active and inactive voxels will be grouped together making the results very difficult to interpret. If the number of clusters is large, the active voxels may be split among various clusters, which may not have any physiological interpretation. Choosing the clustering algorithm is also important. K-means clustering algorithm is the most popular algorithm for fMRI data analysis. Hierarchical clustering methods are also considered because they don't need specifying the number of clusters in advance. A two stage clustering method was proposed in (Filzmoser P, Baumgartner R et al. 1999); the first stage uses a hierarchical approach eliminating the need to specify the number of clusters up front; then the K-means clustering algorithm uses these clusters as the starting point.

3.7 GLM & ICA COMPARISON

Since all the fMRI experiments rely on the detection of small signal changes in the presence of noise, careful statistical analysis is necessary. GLM is a model-based approach where a particular temporal pattern for the fMRI data are hypothesized and imposed into the

model. Though it is highly used and fruitful, if there is no known model for an experiment GLM completely fails. GLM also ignores the differences in the temporal patterns between different brain regions and among different subjects. These issues however don't affect ICA because it does not have any predefined hypothesis or assumptions on the time courses. The only tradeoff with ICA is its complexity, but ICA has become one of the prominent methods for analyzing fMRI data.

3.8 SUMMARY

Due to non-invasiveness, functional magnetic resonance imaging has become an important window to look at the functionality of the human brain. We have presented a brief introduction to the important aspects of fMRI data analysis. It is important to understand the significance of these steps when developing methods for analyzing the data. In the next chapter we introduce methods for analyzing and understanding the activations from the complex fMRI data.

CHAPTER 4

METHODS FOR ANALYZING AND UNDERSTANDING

COMPLEX FMRI

The study of the BOLD activations in the phase has its own significance in one or more ways. The noise in the phase is largely independent to that present in the magnitude and this will be helpful to us in a great deal even if the information is largely convergent. The phase data all by itself also contains information that alone can detect the activations. Since the phase data is relative to the local magnetic field changes, it might contain useful information about the source of the activation. In this chapter we evaluate task-related phase changes compared to the task-related magnitude changes in both block design tasks and event related tasks. We also evaluate the effects of different processing strategies and their influence on the data. We focus on the following main objectives, evaluating the degree to which the voxels are activated in both phase and magnitude, evaluating the degree to which the voxels showed only phase change or only magnitude change, evaluating whether phase changes can be detected in both block and event-related designs and evaluating the effects of additional processing strategies for phase. In addition to addressing the four main objectives, the degree to which the active voxels occur in regions expected to be activated by the task are also evaluated. Before going into the main analysis lets first look at the complexities involved in dealing with the phase data. It is observed that the phase data is often corrupted by the physiological processes, subject motion and other noises. So let's start our discussion with the methods we implemented to reduce/remove these unwanted effects on the fMRI data.

4.1 DEALING WITH PHASE

There are a few aspects of an fMRI experiment that we cannot control, like the scanner-related noise, physiologic variation, head motion etc. The phase is especially sensitive to some of these aspects, so we try to correct for each of these and see if we can improve the activations in phase. The noises generally associated with the fMRI signal are the low frequency scanner drift, high frequency physiological noise and temporally uncorrelated Gaussian noise. To negate the high pass and low pass noises in the data, we try to band pass filter the time courses, and to remove the gaussian noise we try Gaussian filtering. The data is processed for each of these effects and the results are discussed below.

4.1.1. MOTION CORRECTION FOR PHASE

Motion correction realigns the images using a least square approach with a 6 parameter spatial transform(Friston, Frith et al. 1995). A reference image is chosen and all the images in the time course are realigned to match the reference. The header for each input image is modified to show the relative orientations of the data. In general practice, phase fMRI data is not spatially realigned during the initial preprocessing steps. We try to study the effects of realigning the phase. To do this, the 6 spatial transform parameters (x translation, y translation, z translation, x rotation, y rotation and z rotation) are read from the header file for the motion corrected magnitude data and are applied to the phase data. The phase header is updated to show the same relative orientation as that of the magnitude data. Then the data is processed using the GLM approach through SPM. The analysis is performed on the data from the motor tapping paradigm described in Section 3.2.1. The group statistical maps for unrealigned and realigned data are presented in figure 4.1. The results do not show any significant increase in the area or level of activation.

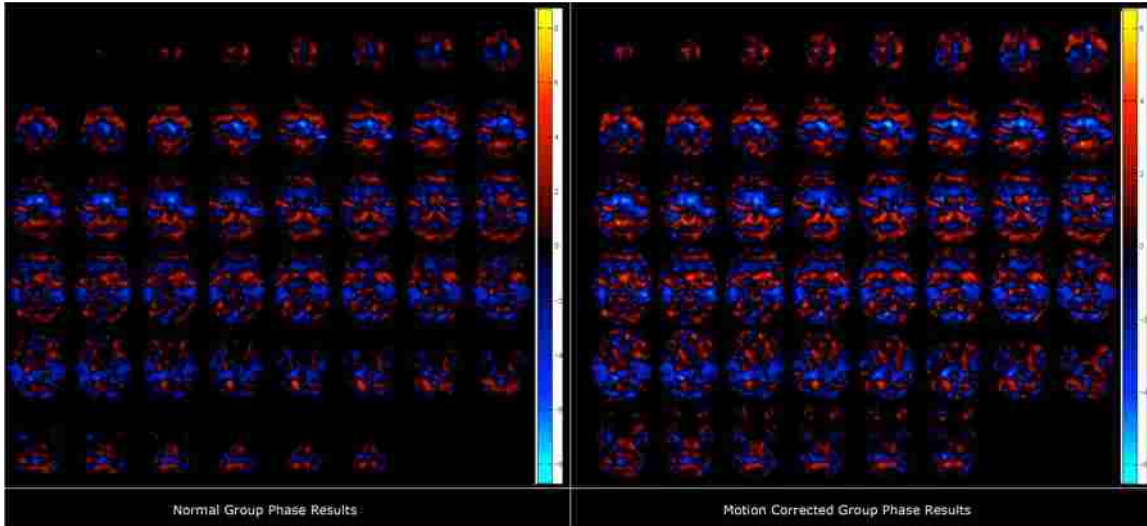


Figure 4.1: Group Activation maps for Normal and Motion Corrected Phase

4.1.2. GAUSSIAN SMOOTHING OF THE TIME COURSES

The general linear model, which can be written as follows, attempts to find the set of experimental parameters (α) for the given design model (M) that best accounts for the original data, (ϵ) is the noise parameter. We try to remove the effects of noise from the measured data by Gaussian smoothing the time courses.

$$Y = \alpha M + \epsilon$$

Measured Data
Amplitude (solve for)
Noise

Design Model

Cf. Boynton et al., 1995

To study the type of noise, we look at the power spectral density of the fMRI signal at two different voxels, one in the region expected to be activated, another in the region not activated by the paradigm and the third is that of a reference signal (model). The plots are presented in figure 4.2.

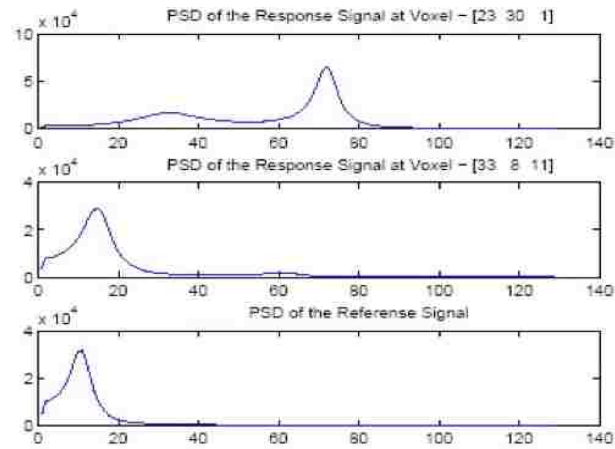


Figure 4.2: a) PSD of the response at a voxel with Noise, b) PSD of the response at a voxel with good response, c) PSD of the Reference signal.

We can say that the noise is Gaussian since it has a random and normal distribution of instantaneous amplitudes over time. Now that the noise is Gaussian at the voxels with no activation, we process each voxel's time course to remove the effect. The frequency response of the Gaussian filter we used is given in Figure 4.2b.

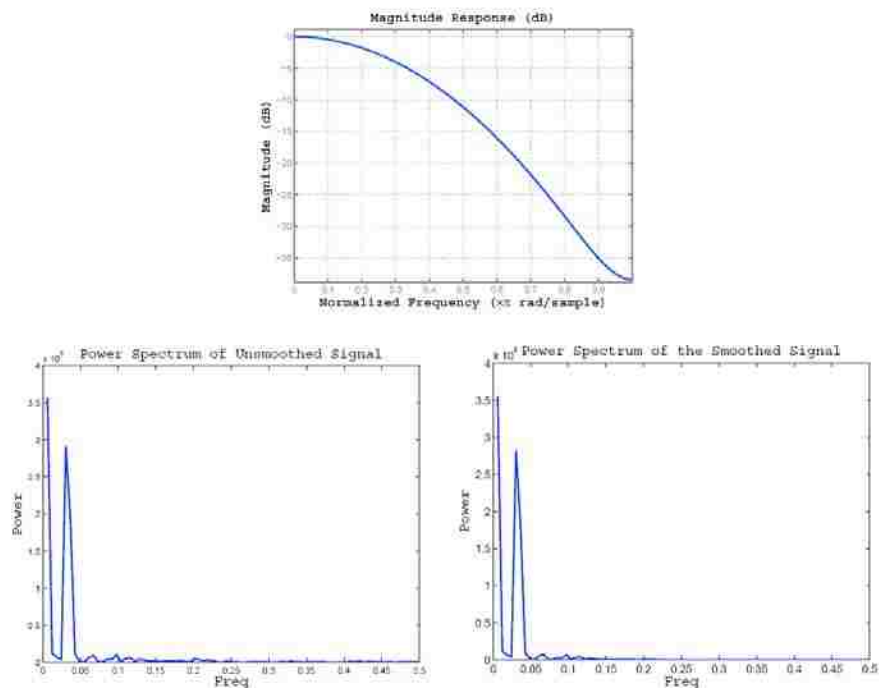


Figure 4.2b: Frequency response of the Gaussian filter.

After filtering the time courses, we reconstructed the data and did the statistical analysis to generate the activation maps. The activation maps with and without Gaussian smoothing are presented figure 4.3.

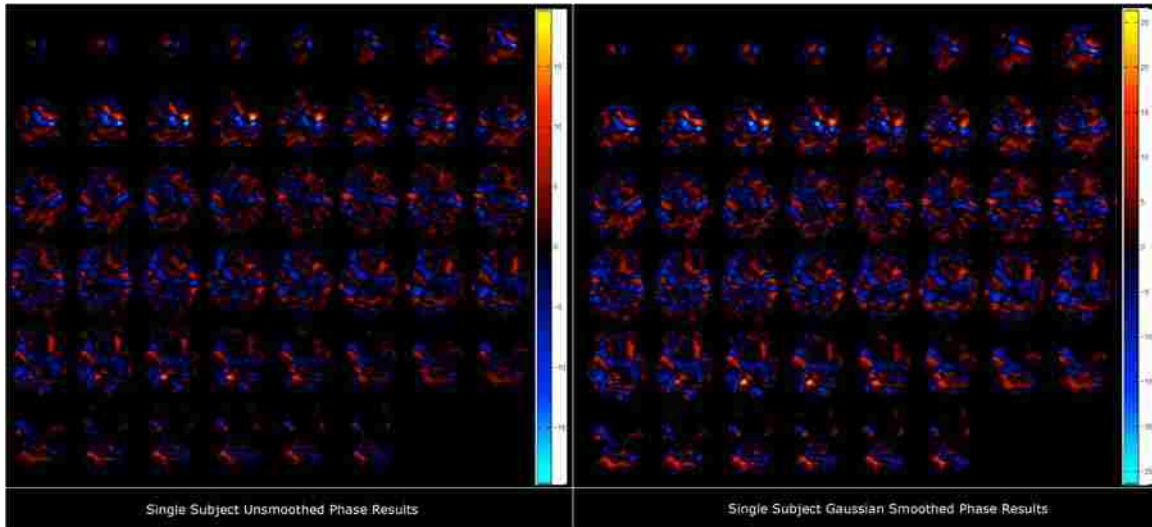


Figure 4.3: Single Subject Activation maps for Normal and Gaussian Smoothed Phase

The smoothed data did not generate larger active regions in phase date, but the peak value in activation improved when compared to that of the unsmoothed data.

4.1.3. COMPLEX DENOISING OF fMRI DATA VIA WAVELET

A fast post-processing method for noise reduction of MR images via wavelet analysis was proposed in (Zaroubi and Goelman 2000). The method is based on shrinking noisy discrete wavelet transform coefficients via thresholding. The MR image is viewed as a two dimensional complex set of $N * N$ observations modelled mathematically, after Fourier transform, as “ $I^{obs} = I + \epsilon$ ” where, $I = I \{x_i, y_i\}$ represents the underlying real or imaginary part of the complex localized signal at position (x_i, y_i) and $\epsilon \{x_i, y_i\}$ is the statistical uncertainty assumed to be Gaussian white noise. We look at the slight modification of the implementation and consider the

phase of the fMRI data to get the underlying real and imaginary parts of the complex localized signal. We try to reproduce the results given in the paper, using the magnitude and phase information from a single subject performing motor tapping paradigm described in section 3.2.1.

As described in the section 2.3, the reconstruction techniques in MRI acquire the data in complex k-space, followed by an inverse discrete Fourier transform (DFT) into complex image space. The signal component of the measurement appears in both real and imaginary channels due to phase errors that are difficult to control. Since the phase errors are difficult to control only the magnitude image is often used. For our analysis we use the MRI acquisition principle to get the complex signal from the magnitude and phase data. We then try to verify the Complex Denoising algorithm on the data. We first convert the phase into radians,

$$Phs = Phs * (\Pi / 2048) - \Pi$$

then calculate the complex signal by using the formula,

$$Complex = Mag. * e^{i * Phs}$$

We then take the Fourier transform of this complex signal to get the underlying real or imaginary part of the complex localized signal at position (x_i, y_i) . To study the noise behavior, we construct the data sorted wavelet spectrum (SWS), which is the amplitude list of the wavelet coefficients ranked in decreasing order. The LogLog plot of the SWS is given in Figure-4.4.

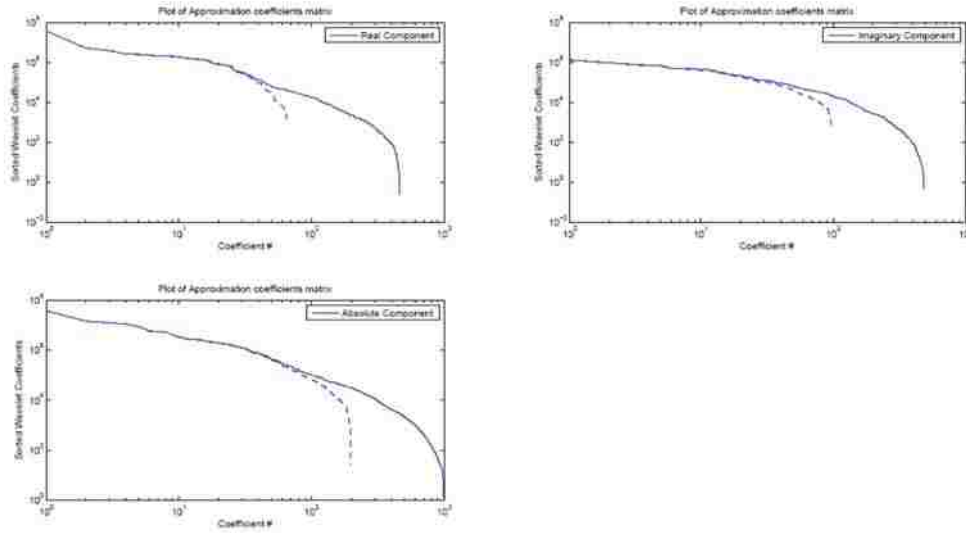


Figure 4.4: Illustration of the wavelet denoising algorithm. In (a) a sorted wavelet spectrum (SWS), of the real component of the data, before (solid line) and after (dashed line) thresholding; (b) the same as in A, but for the imaginary component of the data; and (c) the same as in A, but for the image itself (absolute value).

The paper states that we can expect the break to approximately occur at wavelet coefficients with $SNR \sim 1$, namely; approximately at twice the standard deviation of the background noise, as indeed it is the case here. To calculate the standard deviation of the background noise, we make a mask without the information from the human brain (giving 0 value to voxels in the brain region). We then dilate it with a disk-shaped structuring element, with radius 4. The Dilated mask used in the analysis is given in Figure 4.5. The dot product of the dilated mask and the corresponding 2D information slice gives the area outside the human brain, the standard deviation of this in Discrete Wavelet Transform domain is calculated to get the threshold value of the slice.

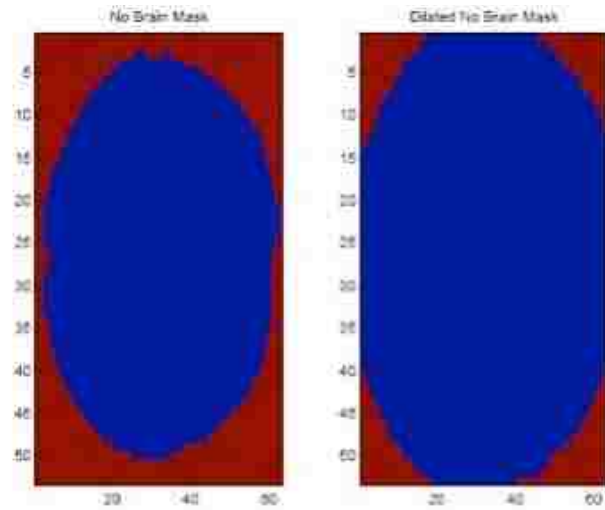


Figure 4.5: Dilated Mask used for Threshold Calculation

Using this threshold, we threshold the Discrete Wavelet Transform of the signal. This thresholding should kill noise prevalent coefficients and keeps only the ‘true’ signal dominated wavelet coefficients. The magnitude and phase are then reconstructed from the processed data. A GLM analysis is done on the reconstructed data through SPM to generate the activation maps. The activation maps for phase before and after complex de-noising are presented in Figure 4.6.

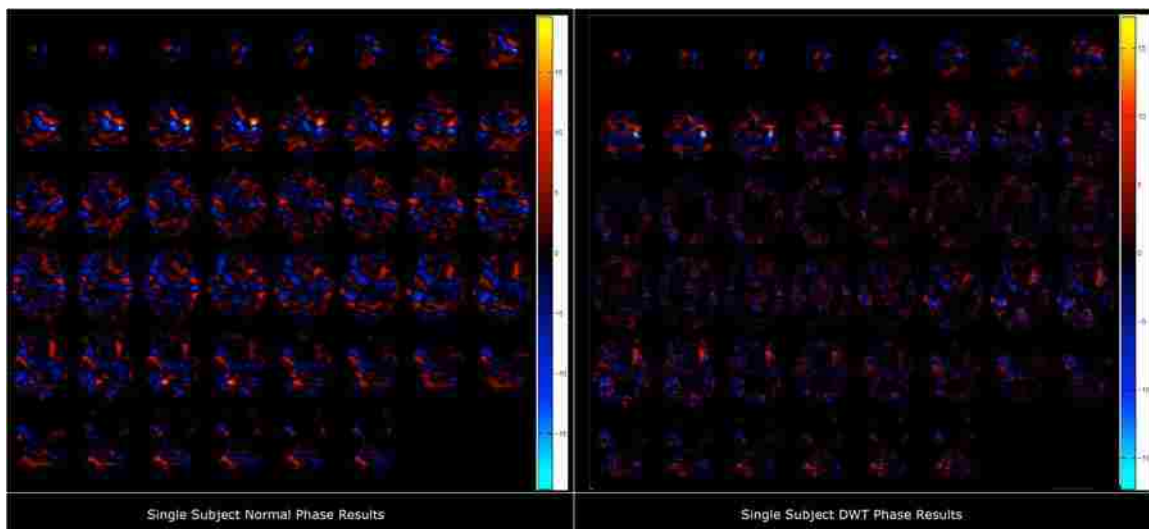


Figure 4.6: Single Subject Activation maps for Normal and DWT De-noised Phase

The results do not show any significant improvement when the complex image is considered (for de-noising). Consideration of the phase information in generating the complex signal gives a more accurate measure of the response signal but did not help much in de-noising the data.

4.1.4. PHASE UNWRAPPING

In fMRI one typically collects a series of complex-valued images,

$$S_k = A_k e^{i\phi_k}, \quad k = 1, \dots, n$$

The phase time series $\phi_k, k = 1, \dots, n$, is typically between $-\pi$ to π and can have phase wrapping. For fMRI analysis the changes from baseline are important and one can subtract the phase of the first image from all the images. The phase change from one image to the next image is typically very small. This subtraction can be done in two ways:

- a) Direct subtraction of phase

$$\theta_k = \phi_k - \phi_1, \quad k = 1, \dots, n$$

If we follow this approach then θ_k will still have phase wrap problems even though the relative change between any scan and the first image is a small number.

- b) Complex Division

We calculate a unit magnitude phase image for the first time point.

$$Y_1 = \frac{S_1}{A_1}$$

Then we can calculate

$$Z_k = \frac{S_k}{Y_1} = \frac{A_k e^{i\phi_k}}{e^{i\phi_1}} = A_k e^{i(\phi_k - \phi_1)}$$

The phase time series can be obtained from the phase of Z_k . For fMRI the phase unwrapping problem is avoided because of small phase images caused by task related activation. In our data sets we do complex division to get unwrapped phase time series.

4.1.5. ISSUES WITH THE PHASE DATA

We have analysed and discussed some of the issues that affect the spatial and temporal stability in fMRI phase time series. The observed phase data is more sensitive to the magnetic field variations. Any magnetic field variations during acquisition related to physiological processes or not, will directly affect phase. The phase data is also very sensitive to all types of noise. It is observed that Gaussian smoothing the time courses (described in section 4.1.2) increases the level of activations in phase statistical maps, but does not improve the area of activation. The temporal filtering which is discussed later (in section 4.4.3) helps remove the non-task correlated effects from the data. It is shown to improve the performance of ICA, but did not help much in the improving the statistical maps for phase. Since the noise effects on phase are independent from those on the magnitude, additional processing might be required for phase data.

4.2. SINGLE SUBJECT ANALYSIS

The main goal of the analysis is to determine which areas of the human brain were active while performing a given task. This can be done using either the General Linear Model or the independent component analysis. To do the single subject analysis in GLM, first the BOLD fMRI response must be modeled, then the parameters must be estimated. Finally the data is

analysed to see if there is any significant increase in the BOLD signal in response to the cognitive task. Independent component analysis takes a more generalised approach by treating the data as summation of several statistically independent signals. Each component has its own activation map.

4.3. GROUP ANALYSIS

In fMRI, it is common to run an experiment multiple times, either on the same subject (having multiple runs for same subject), or on multiple different subjects or both. This will help increase the sensitivity and generalize the conclusion over the population. The main question that arises is, how can we combine the data from multiple subjects? We know that Normalization helps reduce the intersubject variability in the size, shape and orientation of the human brain. Once the data is all normalized to match a standard brain template there are a variety of statistical methods for combining the results across the subjects or sessions. The two most commonly used methods are the fixed-effects analyses and mixed-effect analyses. In fixed-effects analyses, it is assumed that all the subjects activate equally, and is only interested in the within session errors. Mixed-effect analyses also considers the between session errors, so less assumptions are made about the data. The Mixed effect analyses results can be easily generalized to the whole population from which the data is collected. To get the group activation maps, first each subject is motion corrected, coregistered, normalised, spatially smoothed. Then a first level analysis is done on each subject independently to get the statistical maps for each subject. Since all the data is now aligned a second level mixed-effect analysis can be carried out on the first-level statistical maps to test for the differences in activation between the subjects.

4.4. METHODS

4.4.1. WHOLE BRAIN ANALYSIS

A standard GLM analysis was performed on each individual subject using the SPM5 software. Activation maps were computed using a multiple regression framework in which regressors convolved with a canonical hemodynamic response function. A standard GLM of the phase data was performed as well. A random effects group analysis was performed using a voxelwise one-sample t-test applied to the contrast images for each task.

4.4.1.1. WHOLE BRAIN ANALYSIS FOR MOTOR TAPPING

Activation maps were computed using the multiple regression framework within SPM5 in which regressors are created from the stimulus onset times and convolved with a standard hemodynamic response function. A contrast was created for each individual subject for finger tapping versus rest. To compute the group maps a second level analysis was performed using the activation maps from each individual subjects and entering them into a one-sample t-test. The highest magnitude change was observed in the motor cortex.

4.4.1.2. WHOLE BRAIN ANALYSIS FOR AUDITORY ODDBALL

The same multiple regression framework within SPM5 was used here. The regressors for each participant's fMRI model were derived by extracting stimulus onset timings for all target, novel, or standard stimuli for AOD. Different Contrasts were specified to evaluate the effects of target stimuli relative to the standard stimulus baseline; novel stimuli relative to the standard stimulus baseline; target stimuli versus novel stimuli; novel stimuli relative to target stimuli; and standard stimuli relative to the implicit baseline. To compute the group maps a second level

analysis was performed using the novels vs. standard activation maps from each individual subjects and entering them into a one-sample t-test. The highest magnitude change was observed in the motor cortex and the temporal lobes for target stimuli and in the temporal lobe for novel stimuli.

4.4.1.3. RESULTS AND DISCUSSIONS

Figure 4.7 shows the magnitude change and phase change of the results for motor tapping and auditory oddball. The highest magnitude change for motor tapping was observed in the motor cortex and for the auditory oddball highest change was in the temporal lobe for novel stimuli. Maximal phase changes were also observed in motor cortex for MT and in temporal lobe for AOD. The plots in the top-right and bottom-right panels in the figure are the RGB maps for MT and AOD. The areas in red are where only magnitude activations were observed, the ones in green are for phase only activations and the areas in blue are where both magnitude and phase activations were observed. The resulting activation changes for phase and magnitude data for both motor tapping and AOD were cluster thresholded to correct for multiple comparisons at $p < 0.05$ (FWE).

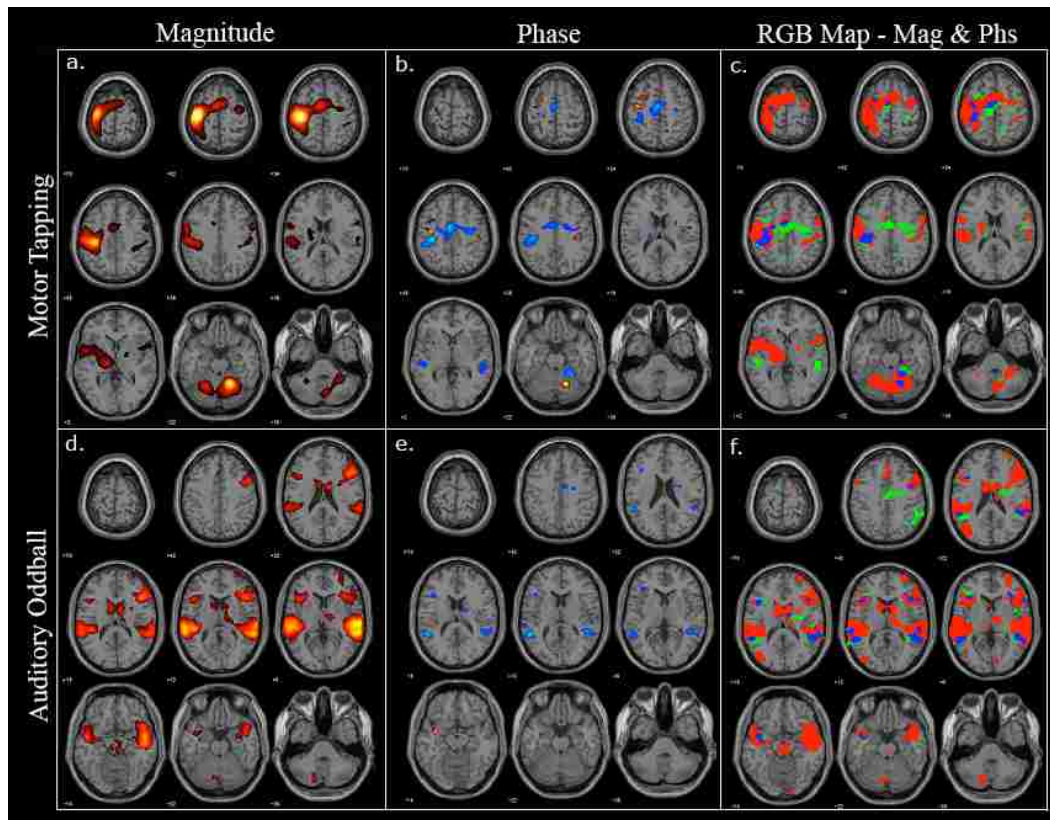


Figure 4.7: Whole Brain Analysis Results

The second level analysis, on the t-maps of individual subjects, was performed for whole brain analysis at the group level. The maps presented in the results show that there are quite a few voxels that are activated in both phase and magnitude. The color maps in Figure 4.7 show the voxels that showed only phase change or only magnitude change and both phase and magnitude activations in different colors. The maps present the fact that the active voxels occurred in regions that are expected to be activated by the task. The maps also put forth the fact that there is phase activation in the expected regions where the magnitude activations are insignificant. Our study demonstrates that phase activation is present in both block and event-related design. It was found that the preprocessing details, such as masking, temporal filtering and cluster removal significantly impact the results.

4.4.2. ROI ANALYSIS: TIME LOCKED AVERAGING

The whole brain analysis looks for significant activations in many different voxels covering the entire brain. If we are interested in a particular region of the human brain, we can use more targeted analysis approach like the region of interest (ROI) analysis to see the pattern of activity that occurs in that region. Time locked averaging is a widely used technique for ROI analysis. The technique is based on simple signal averaging theory proposed by Lynn, P. A. in his book (Lynn 1989). In our case of a simple block design experiment like the MT, the response is observed to be a repeated signal as shown in Figure 4.8a.

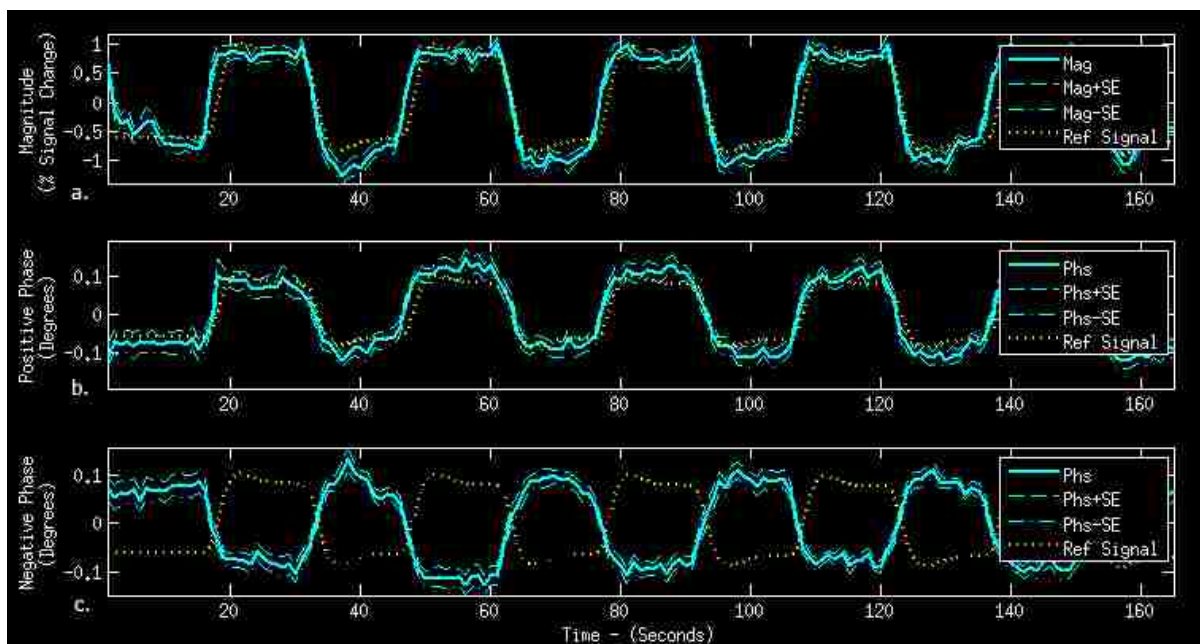


Figure 4.8: Magnitude and phase fMRI time courses for MT

The time series shows activations at different onset times. The time series is split at each onset time and the average of the resultant time courses is calculated to create a response for each subject. Any fMRI time series mainly contains two components, a genuine response signal, and random fluctuations due to uncorrelated physiological events and noise in the image. Time

locked averaging also helps in reducing the magnitude of the noisy component, but the information in the repetitive signal is preserved. The noise in the signal was filtered before time locked averaging is done on it. A band pass digital Butterworth filter of order 8 with pass band [.05 .7] was used to filter the time courses before further processing was done. In our analysis, the regions with possible activation were determined from the experimental paradigm and the voxels present in that particular region were considered for the analysis. The top 10% of the voxels that had the maximum/minimum values were studied. Time locked averaging was performed on each of these individual voxels; this produced an individual time course. The mean of the results for each voxel was computed and considered as the resultant time course for that subject. The final time course was the averaged time course across all the subjects. The standard error across the subjects was computed to see if there is any discrepancy among the subjects.

4.4.2.1. MASKING

The software package wfu_pickatlas (<http://fmri.wfubmc.edu/cms/software#PickAtlas>) was used to create the masks for each analysis. For motor tapping, a mask was created by selecting Brodmann areas 3, 4 and applying a single 3D dilation. For auditory oddball, the region of interest was the temporal lobe, the mask was created from the temporal lobe and applying a single 3D dilation via wfu_pickatlas.

4.4.2.2. ONSET TIMES

During a typical block design fMRI experiment, the blocks are presented with periods of 30 s OFF and 30 s ON. The subject taps his/her fingers during the ON period and rest during the OFF cycle. During the on cycle the brain regions involved in hand and finger movement is

active, and the activity returns to baseline during the off cycle. The time at which the stimulus is presented plays a very important role in any analysis. The time instances when the stimulus is presented are called the onset times. For the event related tasks like AOD, different stimuli (targets and novels) are presented at different times each of which have their own onset times.

4.4.2.3. ROI FOR MOTOR TAPPING

Time locked averaging (TLA) was performed on the individual subjects for MT. The fMRI time courses were split based on the onset times and the average of the time courses at each onset time was calculated to get the final TLA course of that individual subject. This was performed on all the seventeen subjects. Then the mean TLA across the subjects was calculated to get the final time locked average for motor tapping. TLA was done on both magnitude and phase data to see if the activations were consistent with each other. Standard error was also calculated to verify the variance across the subjects.

4.4.2.4. ROI FOR AUDITORY ODDBALL

The TLA on the AOD data was performed by extracting stimulus onset timings for all targets. These target onsets were used to split the time courses in each subject and the average was calculated to get the response of the subject. All thirty four subjects were analyzed and mean across the subjects for both magnitude and phase were calculated. TLA plots along with the standard error were analyzed, and the activations in both magnitude and phase data were consistent with each other.

4.4.2.5. RESULTS AND DISCUSSIONS

The time locked averaging results for motor tapping and the spatial locations of the voxels are presented in Figure 4.9. We show TLA results for voxels which had maximum magnitude response (Figure 4.9a), the corresponding anatomical map (Figure 4.9b) displaying the voxels with the maximum magnitude response considered for the analysis, TLA results for voxels which had maximum positive (Figure 4.9c) and negative (Figure 4.9e) phase response, and TLA results for voxels significant positive (Figure 4.9d) and negative (Figure 4.9f) phase response with insignificant magnitude response. The dotted lines are mean response \pm standard error. Thus, as has been shown previously the phase response can be positive and negative in different spatial locations, these locations of maximum phase response do not coincide with those of maximum magnitude response, and finally we have statistically significant phase response in regions where the magnitude response is not significant presented in figures 4.9(g,h,i,j).

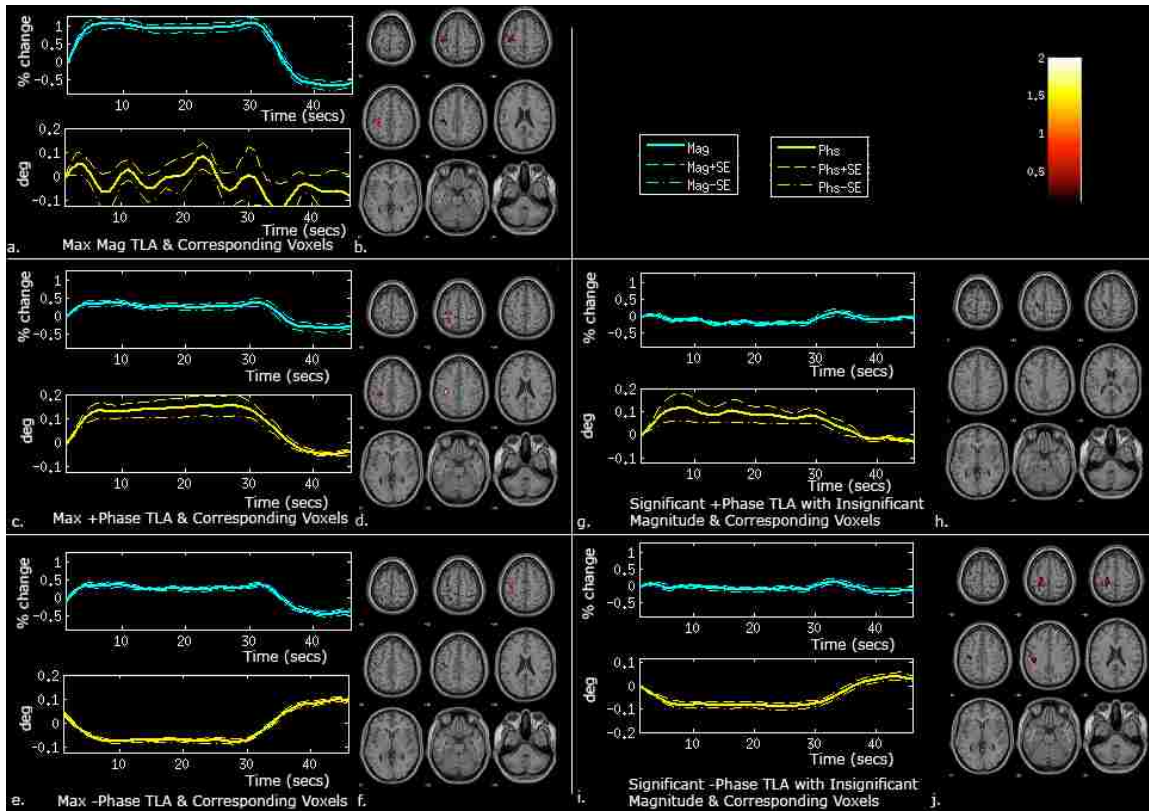


Figure 4.9: Group Time Locked Averaging Results for Motor Tapping

Figure 4.10 is similar to Figure 4.9 and shows the time locked averaging and the corresponding anatomical maps for auditory oddball novel stimuli. We focused only upon the novel stimuli in this study since novel stimuli are a robust activator of temporal lobe.

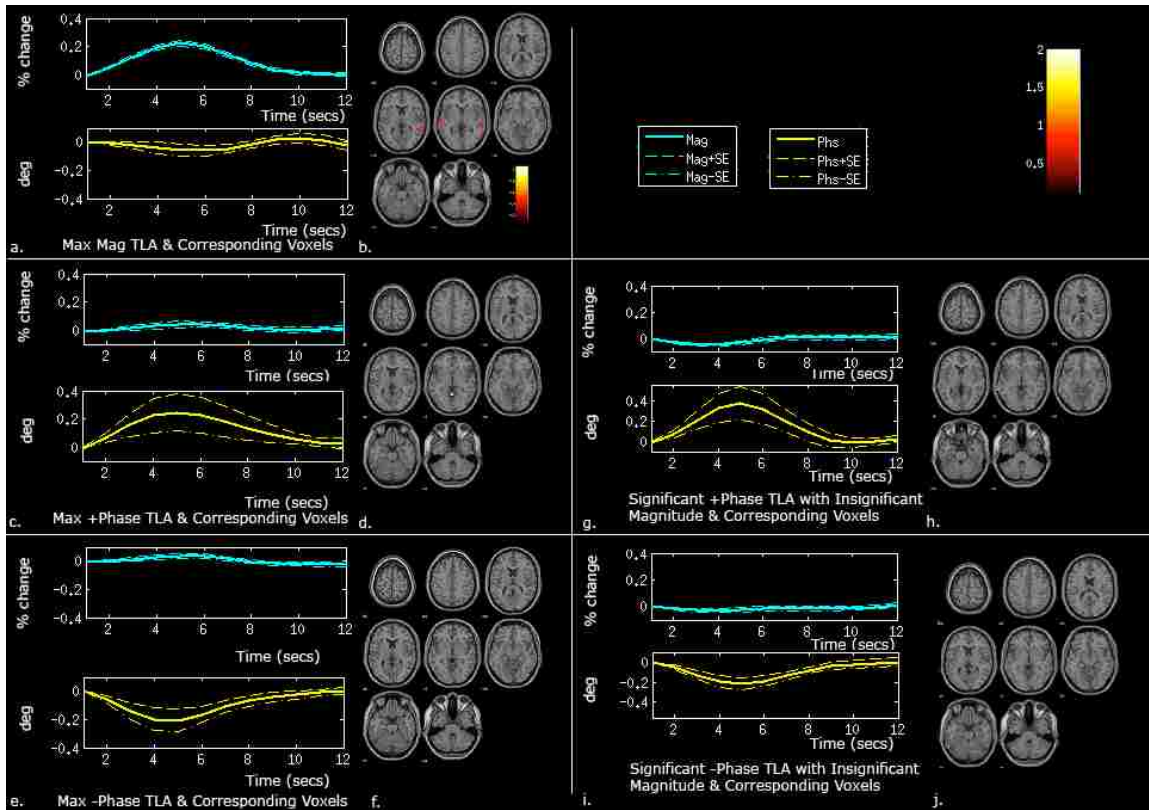


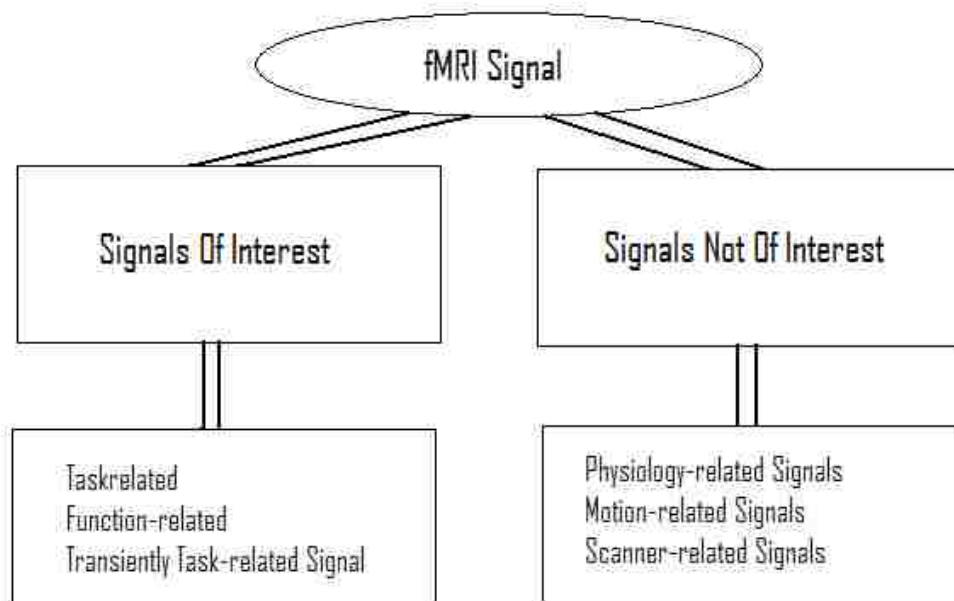
Figure 4.10: Group Time Locked Averaging Results for AOD

With ROI analysis, the patterns of activation in a particular neural region predicted to covary with the task of interest were studied. The motor tapping (MT) data and auditory odd ball (AOD) showed activations as expected. The positive and negative phase activations are present for both the MT and AOD tasks. At the voxel with highest magnitude change, a randomly fluctuating phase signal was observed in the group. The voxel with maximum positive/negative phase showed significant magnitude activation suggesting that the phase activations are concurrent with magnitude activation. Some of the voxels in the regions expected to be activated, showed significant phase changes with no observable magnitude changes, which suggests that phase data may hold useful information. The standard error plots confer the fact that the phase

showed consistent activation across the subjects in the group. Our results also show that the changes in phase are consistent with those observed in magnitude.

4.4.3. TEMPORAL FILTERING & ICA

The fMRI data is effected by various kinds of noise like thermal noise responsible for variation in background Eddy currents, scanner heating, power fluctuations typically caused by scanner problems, head motion effects, physiological changes, differences across brain regions like functional differences and Large vessel effects and last of all the artifact-induced problems. We try to negate the effects of some of these unwanted sources. The fMRI signal can be decomposed as follows:



Independent component analysis can be used to discover the sources that are maximally independent from the observed data and to differentiate the signals of interest from the signals not of interest. Our goal is to analyze how temporal filtering of data effects ICA. That is if high

frequency and low frequency noise are filtered out (before doing ICA), we can expect to see some improvement in correlation values.

The goal is to preserve signal frequencies of interest (those elicited by design) while removing low and high frequency noise (not elicited by design). The low frequency noise shifts the baseline and can be due to machine drift. Removing this may help us optimally fit the signal components of interest in the study. The high frequency noise impacts temporal SNR especially for short duration activations and short design blocks.

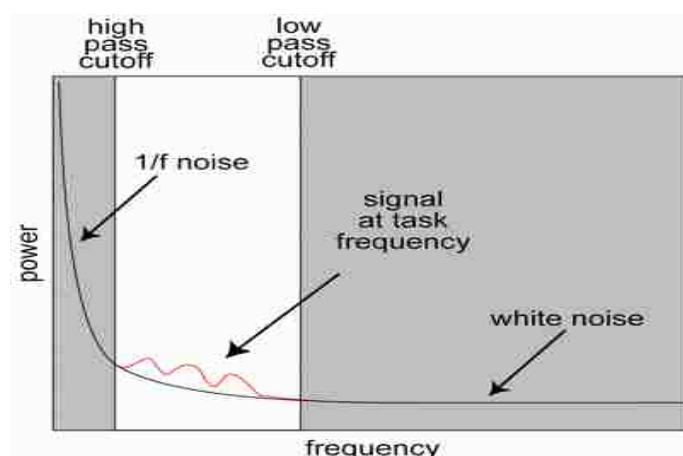


Figure 4.11: Power Spectrum of the fMRI time course

If we look at the power spectrum of the signal show in figure 4.11, we can typically segment it into three parts. The first region will be the power at low frequencies; the power can probably be even more than shown here - the lower the frequency the more power. The second region at higher frequencies, where the power does not vary with frequency, we refer to this as white noise. The third region depicted in white is the ideal band of frequencies and our signals of interest will be around this area shown in the red line. Our goal is to attenuate the gray areas that depict the frequencies of unwanted signal.

4.4.3.1. STRINGENT BAND PASS FILTERING

A simulation was done to see how temporal filtering affects our data. We consider the reference to be as shown in figure 4.12a. The low frequency drift and high frequency noise are modeled as shown in Figure 4.12b, figure 4.12c respectively. The raw signal is the summation of the low frequency drift (this can typically be non linear), the high frequency noise and the reference signal, as shown in Figure 4.12d.

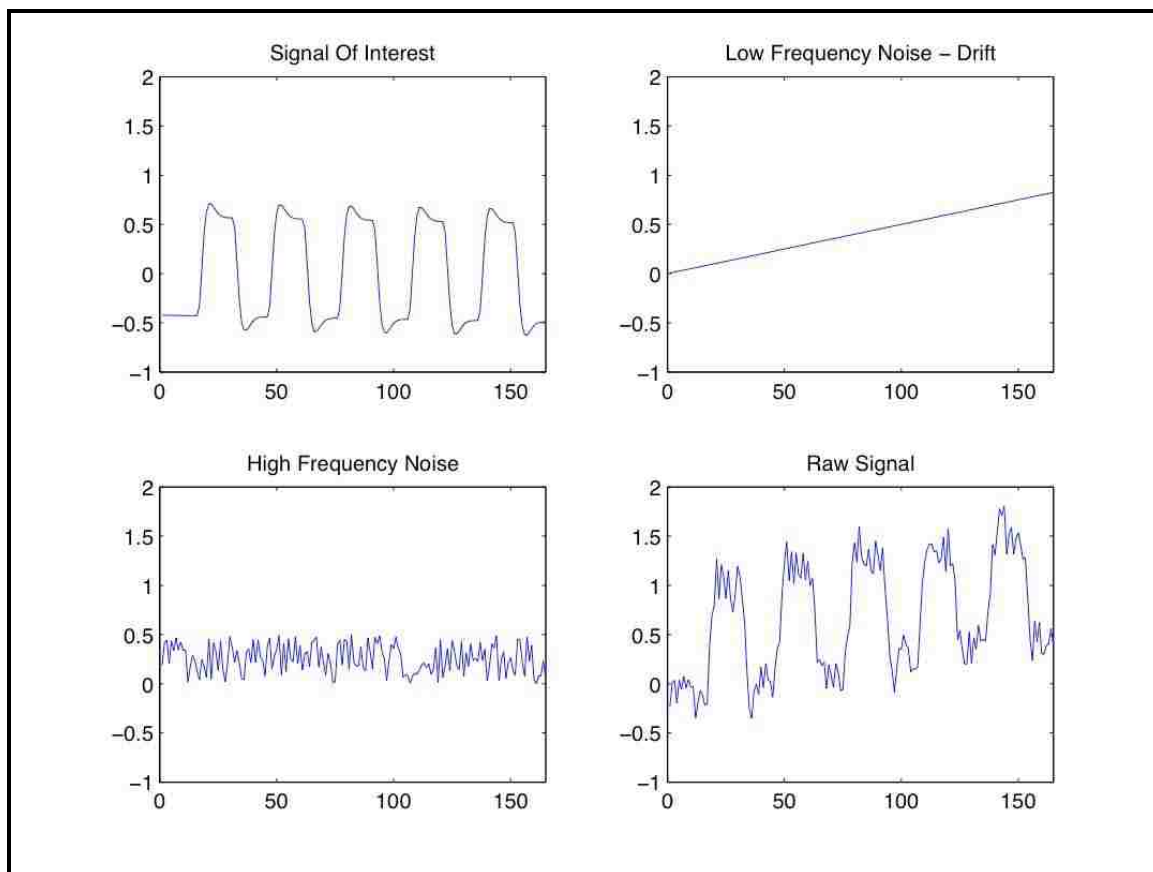


Figure: 4.12: Temporal filtering simulation

This raw data is filtered to get back to our signal of interest. To attenuate the Low frequency drifts and the high frequency noise the filter is defined as a band pass filter. The low-pass filter cutoff would typically correspond to the Nyquist frequency or rate. For example, if we

have a TR of 2 s, which is $f=0.5\text{Hz}$, the fastest signals we can measure occur at $1/2f$ or 0.25Hz . The high-pass filter cutoff would correspond to the slowest signal we wish to measure. Typically, this is equal to the longest whole trial (i.e., start of trial to start of next trial). For example, say our longest trial is 20 s, which is $1/20 = 0.05\text{ Hz}$, so the high-pass cutoff will be 0.05Hz .

For the data that was modeled in the simulation, we calculate the high pass and low pass cutoffs. The TR for our data is 2seconds, so the low-pass cutoff will be 0.25Hz . The longest whole trail is 15seconds, so the high-pass filter cutoff will be $1/15$. If we attenuate the raw signal using strict cutoffs our output will be as shown figure 4.13.

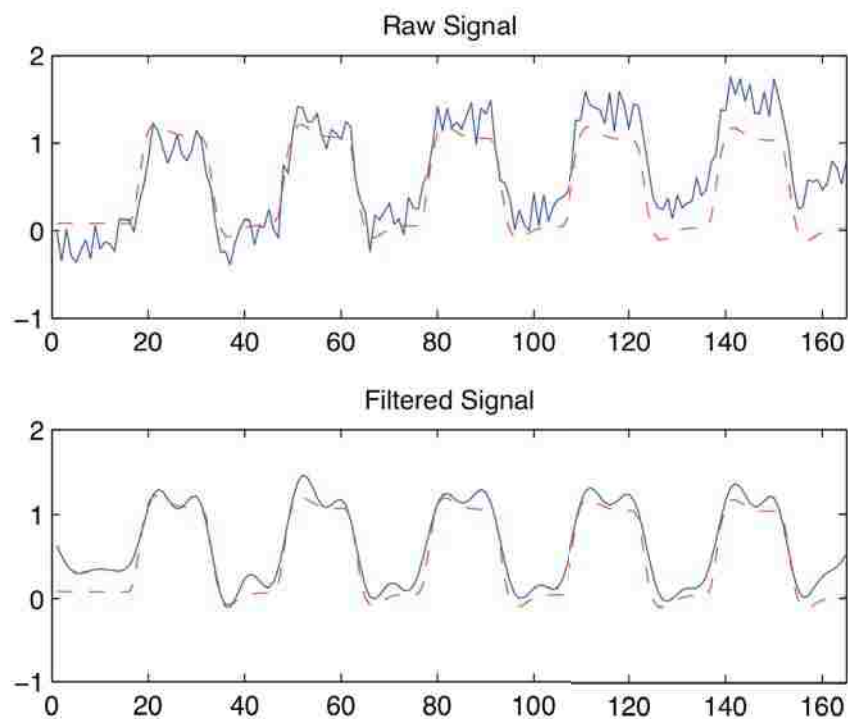


Figure 4.13: Raw and band pass filtered time courses

4.4.3.2. EFFECTS ON ICA

To do such strict cutoff we need the information about the design matrix. The main advantage of ICA is that it can separate the sources without any information about the design matrix. It is preferred that the filtering parameters be more generalized to fit any design task and produce a considerable improvement. For our analysis a generalized filter was used, whose frequency response is shown in figure shown in figure 4.14.

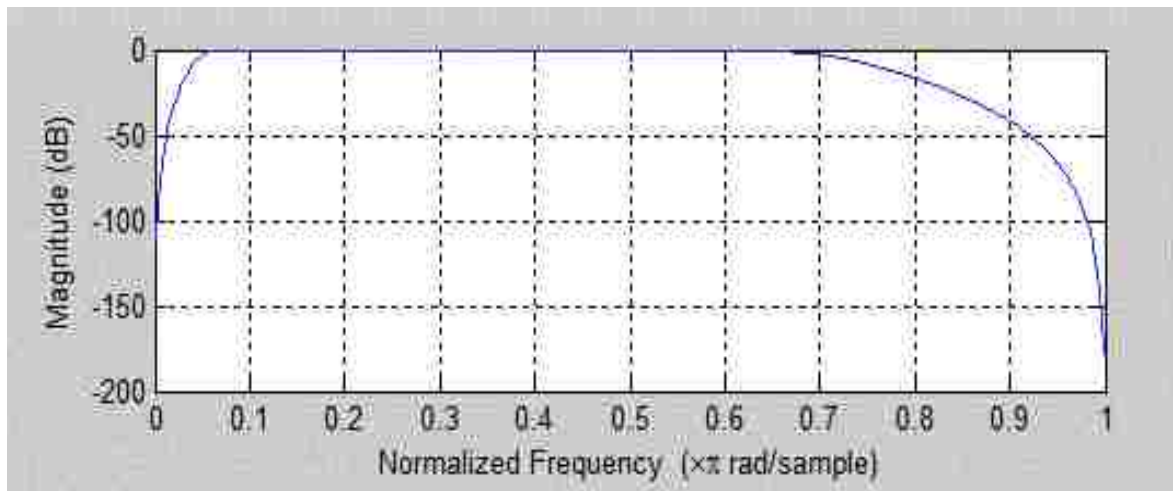


Figure 4.14: Frequency response of an 8th Order bandpass Butterworth filter with pass-band from 0.05 to 0.7Hz.

The data was filtered using these parameters. The results are presented in Figure 4.15, they show a significant reduction in the high frequency noise and the low frequency noise is completely zeroed out. The filtered data fits better with the reference signal compared to the unfiltered signal.

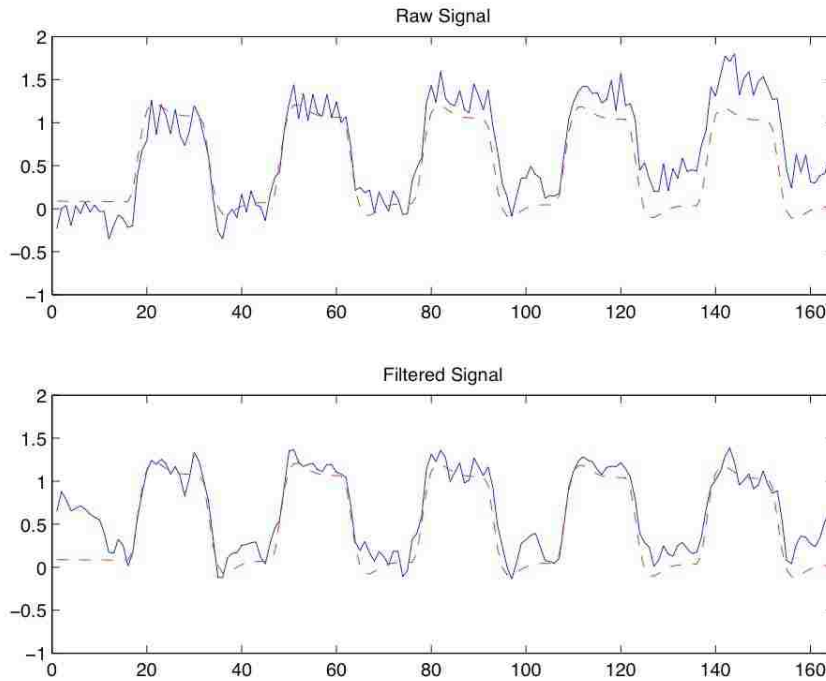


Figure 4.15: Raw and band pass filtered time courses for the generalized parameters

4.4.3.3. RESULTS & IMPROVEMENT

The simulation results were encouraging, so we implement the filtering on real time fMRI data. Our data is from a motor tapping (MT) paradigm; a block design with periods of 30 s OFF and 30 s ON. The subjects tapped their fingers during the ON period and rest during the OFF cycle. There were five and a half cycles, starting with OFF and ending with the OFF period. 165 whole head fMRI images were collected for each subject. The total experiment time was 5.5 minutes. We analyzed the data from 16 healthy subjects that participated in the motor tapping experiment. The real-time fMRI time course from one of the subjects was filtered, to see how it affects the data. The plots for unfiltered and filtered data are presented in the figure 4.16. Both low frequency drift and high frequency noise can be observed in the unfiltered data. Temporal

filtering seems to have reduced these effects because the filtered time course fits better with the reference signal compared to the unfiltered time course.

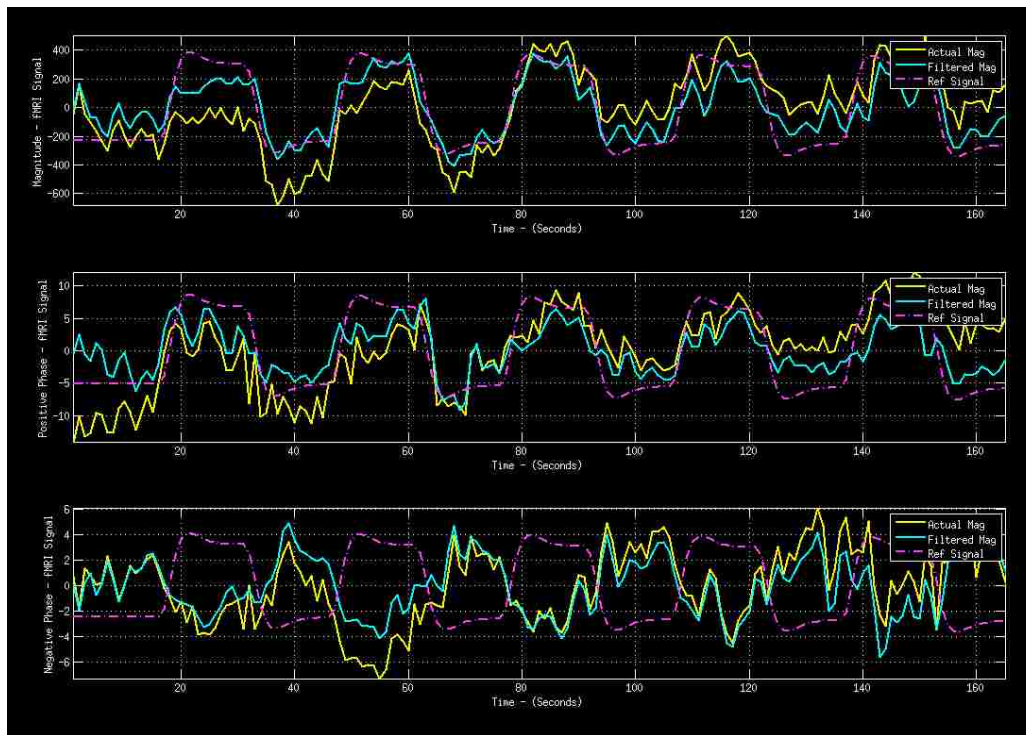
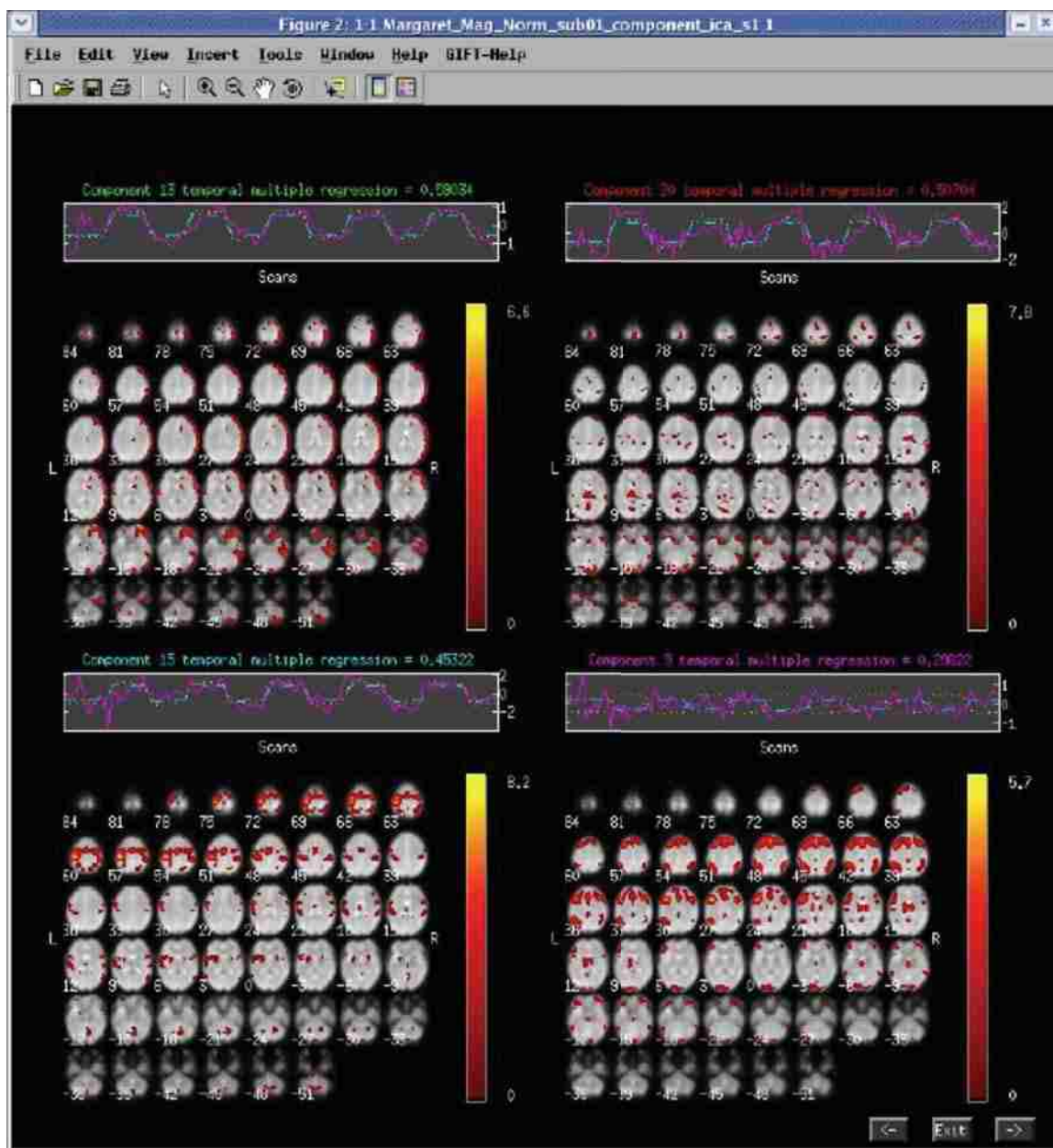


Figure 4.16: Effects for temporal filtering on real time data

Independent component analysis was performed on the data. The results of ICA for both unfiltered and filtered data are presented in figures 4.17 and figure 4.18 respectively.



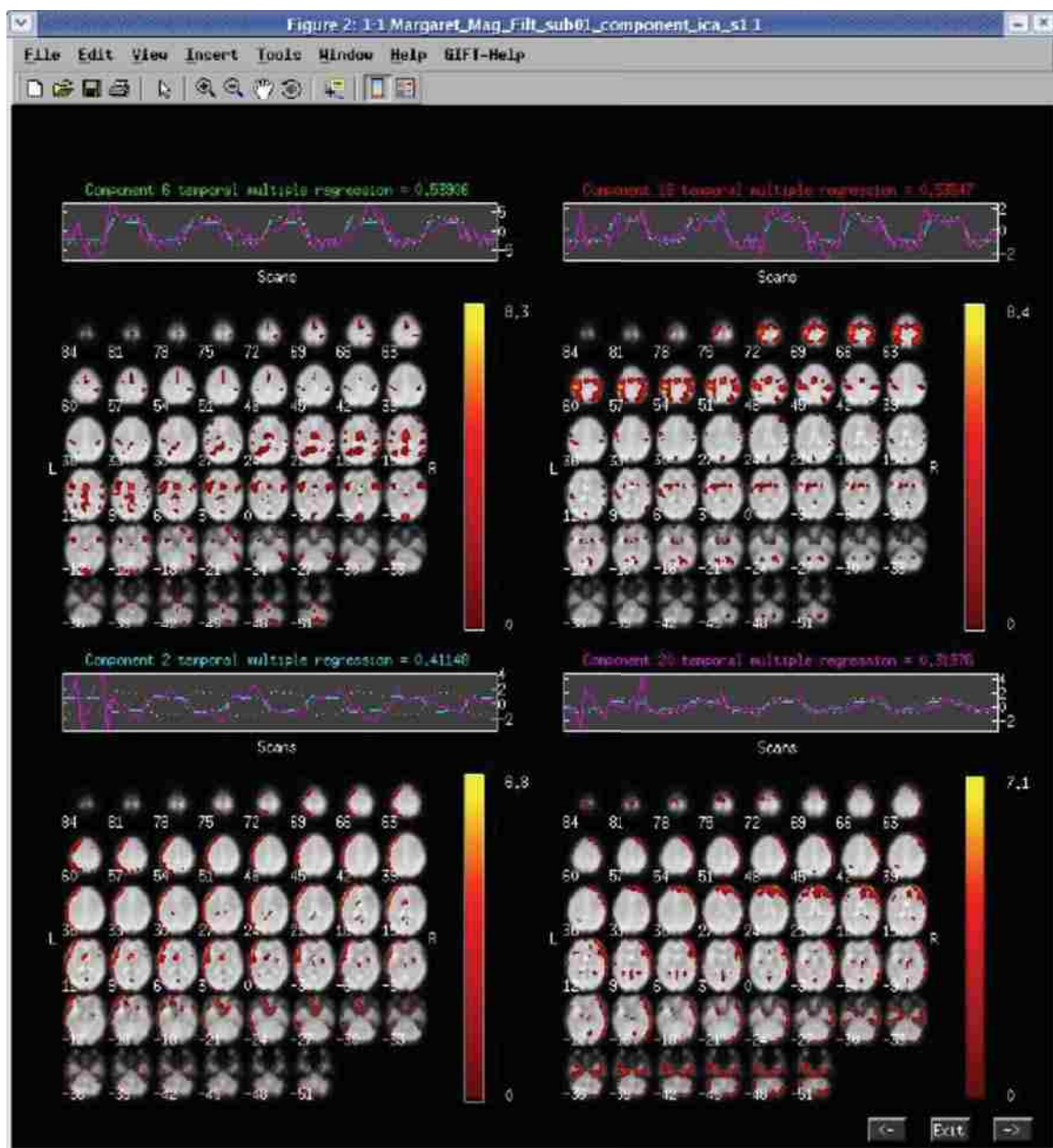


Figure 4.18: ICA results for Filtered Data

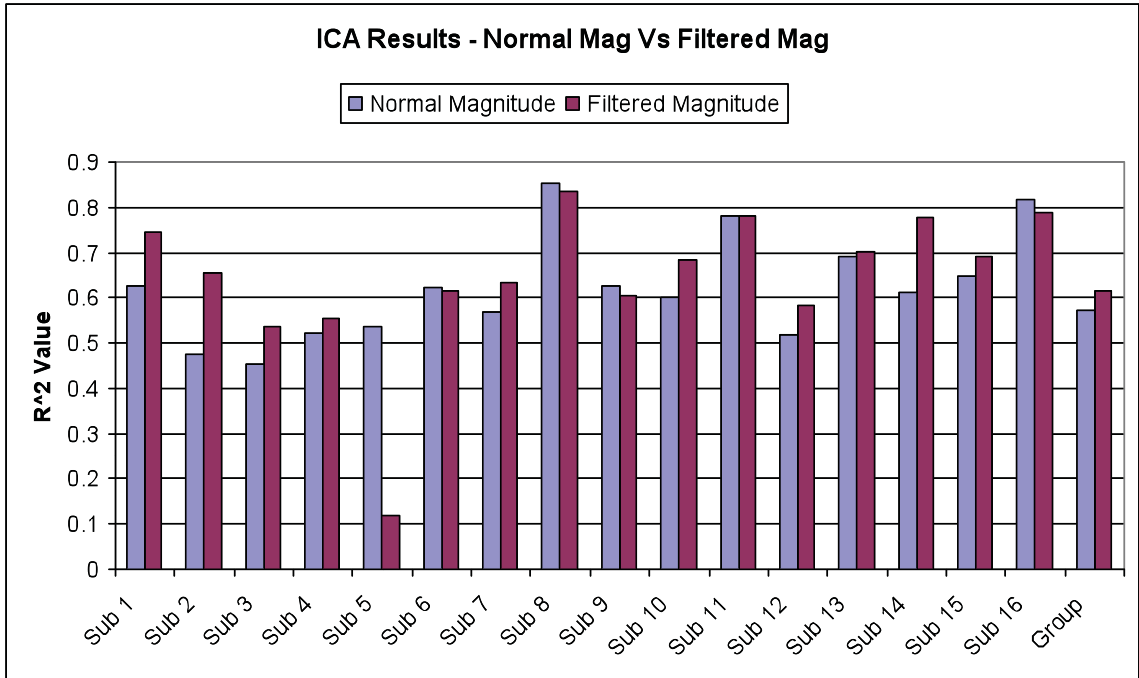


Figure 4.19: Bar plot of how Individual and Group ICA reacted to Temporal Filtering of Magnitude

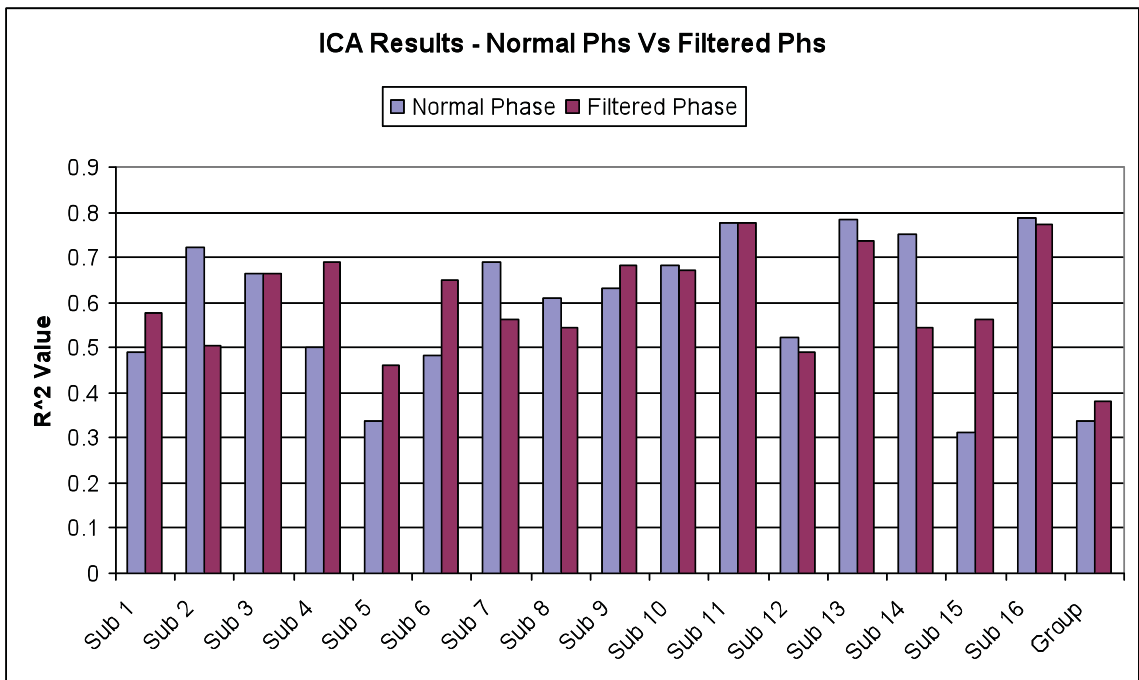


Figure 4.20: Bar plot of how Individual and Group ICA reacted to Temporal Filtering of Phase.

4.4.3.4. DISCUSSIONS

Our main goal was to study how temporal filtering affects the data and so the ICA. We tried to identify the unwanted frequency variation like the Drift (low-frequency) and Physiology (high-frequency) noise, reduce power around those frequencies through application of filters. Looking at the ICA results for the single subject, shown in figures 4.17 and 4.18, it can be observed that the unfiltered magnitude ICA (figure 4.17) gave a partial correlation value of 0.45322 for our component of interest that is the motor cortex. ICA of the filtered magnitude data (figure 4.18) produced a partial correlation value of 0.53547 (with nearly an 18.14% increase in the correlation values) for our component of interest. An increase in the volume of activation was also observed in the component of interest. The magnitude bar plot showed in figure 4.19 gives us a generalized result on how temporal filtering affects the ICA. Most of the subjects showed a good increase in the activation (correlation values). This suggests us that temporal filtering helps ICA.

The results suggest that it is advantageous to do the temporal sorting on the data before inputting it into GIFT (Group ICA of fMRI Toolbox). This helped increase the detection efficiency of ICA Infomax algorithm (for most of the subjects). Since our cutoff was much generalized, it didn't boost-up the results very high, but if we use more stringent cutoff it might help our case. To do a more stringent cutoff we need to consider the experimental paradigm or the design matrix which compromises the credibility of ICA. So given a particular data, we need to develop methods to actually calculate the cutoff values with out looking into the design matrix. Finally we can come to a conclusion that temporal filtering does improve the ICA results (for almost all the subjects) but more work is needed to do a better job on each and every subject.

4.5. SUMMARY

The goal of our analysis was to verify the presence of phase activations in both block and event-related design studies and if so, to determine if these changes were in regions expected to be involved in the tasks. The secondary goal was to understand the properties of phase data to see if any special preprocessing steps for phase were necessary. The phase information at a group level for two different paradigms was analyzed. The result from both the ROI analysis and the whole brain analysis show phase activation in the expected regions where the magnitude activations are insignificant suggesting that the phase data might hold useful information. Different processing steps were implemented and their effect on the phase data was studied. A Talairach analysis was also performed in the data to analyze the results. The statistical maps were studied with all the regions of interest in the human brain; Table 1 represents the peaks of activation for MT data for magnitude and phase and their corresponding talairach coordinates. Table 2 represents the peaks of activation for AOD data and the corresponding talairach coordinates.

Table 1: Talairach table for motor tapping

	<i>Area</i>	<i>Brodman Area</i>	<i>L/R Volume</i>	<i>L/R random effects: Max T (x, y, z)</i>
<i>Magnitude</i>	Precentral Gyrus	4, 6, 44	4.8/20.6	4.4(-56,5,36)/14.9(39,-15,56)
	Postcentral Gyrus	3, 4, 2, 40, 1, 5, 43, 7	3.6/15.8	3.3(-50,-21,37)/13.9(42,-18,53)
	Cerebellum		29.3/12.9	13.8(-21,-53,-18)/7.3(24,-56,-17)
	Middle Frontal Gyrus	6, 9, 8	2.7/6.3	4.4(-56,2,39)/11.6(30,-9,61)
	Superior Frontal Gyrus	6	2.8/3.8	5.7(0,6,52)/11.5(33,-8,64)
	Medial Frontal Gyrus	6, 32	3.2/4.7	6.4(0,3,52)/7.4(6,0,53)
	Fusiform Gyrus	19, 37	0.9/NA	6.7(-21,-56,-10)/NA
	Inferior Parietal Lobule	40	0.6/5.6	3.1(-36,-30,40)/6.7(45,-30,46)
	Cingulate Gyrus	24, 31, 32	1.2/2.5	5.3(0,2,47)/6.3(6,-1,47)
	Culmen of Vermis		0.3/0.1	6.3(-3,-65,-9)/4.0(3,-65,-9)
	Thalamus		NA/4.9	NA/5.8(15,-17,4)
	Inferior Frontal Gyrus	9, 44, 45, 47	2.1/2.3	4.3(-56,7,33)/5.5(59,7,27)
	Lingual Gyrus	18, 19	1.2/0.1	5.0(-18,-70,-9)/2.7(3,-76,-6)
	Lentiform Nucleus		0.7/5.4	2.8(-21,-3,-2)/4.9(21,-6,-5)
	Insula	13, 40	0.5/5.7	2.9(-45,9,-3)/4.8(48,3,3)
	Superior Temporal Gyrus	22, 41, 38, 42	1.5/4.1	3.1(-48,9,-3)/4.6(50,3,0)
	Paracentral Lobule		NA/0.1	NA/3.8(6,-9,47)
	Superior Parietal Lobule	7, 5	NA/1.2	NA/3.8(30,-47,60)
	Precuneus	7	NA/0.1	NA/3.3(30,-47,52)
	Parahippocampal Gyrus		NA/0.2	NA/3.0(27,-4,-12)
Transverse Temporal Gyrus	41, 42	NA/0.6	NA/3.0(56,-17,12)	
Lateral Ventricle		NA/0.1	NA/2.6(24,-15,-7)	
<i>Phase Positive</i>	Precentral Gyrus	6, 43, 13, 9	1.3/1.9	4.0(-39,-19,34)/4.8(36,-12,45)
	Middle Frontal Gyrus	6	0.2/2.1	2.8(-33,6,52)/4.7(33,-12,45)
	Cerebellum		2.5/NA	4.7(-18,-62,-15)/NA
	Postcentral Gyrus	3, 2	1.1/NA	3.7(-39,-16,31)/NA
	Precuneus	7,31	0.6/0.2	3.2(-15,-50,49)/2.7(3,-59,44)
	Cingulate Gyrus	31	0.2/0.1	3.2(-15,-42,27)/2.8(12,-42,27)
	Superior Temporal Gyrus	22	0.1/0.1	2.6(-50,-3,3)/2.9(50,-11,9)
	Medial Frontal Gyrus	6	NA/0.2	NA/2.8(9,8,52)
	Superior Frontal Gyrus	6	NA/0.2	NA/2.8(6,8,52)
	Insula		0.1/0.2	2.6(-45,-11,17)/2.7(45,6,-3)
<i>Phase Negative</i>	Postcentral Gyrus	3, 2, 40, 5	0.9/5.9	2.2(-50,-30,35)/7.9(33,-24,43)
	Cingulate Gyrus	24, 31, 32, 23	6.9/8.9	6.9(0,-7,45)/7.3(3,-7,45)
	Paracentral Lobule	31, 6	0.4/1.5	6.5(0,-9,47)/7.1(3,-9,47)
	Medial Frontal Gyrus	6, 10, 32	2.1/4.7	5.8(0,-9,50)/6.6(3,-9,50)
	Precentral Gyrus	4, 6	5.9/2.8	4.3(-36,-10,42)/6.2(39,-21,37)
	Cerebellum		6.1/2.6	5.8(-27,-44,-15)/2.8(24,-42,-21)
	Parahippocampal Gyrus	37, 19, 36, 28, 30	1.9/1.4	5.5(-21,-47,-10)/3.7(36,-33,-11)
	Inferior Parietal Lobule	40	2.8/6.7	2.3(-42,-36,46)/5.5(45,-25,29)
	Fusiform Gyrus	37, 19, 20	2.5/1.9	4.3(-21,-53,-7)/3.6(36,-36,-11)
	Middle Temporal Gyrus	22, 21, 37, 39	7.9/3.7	4.0(-56,-35,-1)/2.6(48,-32,2)
	Middle Frontal Gyrus	6, 11, 9	1.3/0.3	4.0(-30,-12,45)/4.0(24,-7,45)
	Superior Temporal Gyrus	41, 22, 42, 21, 39, 13	7.1/8.4	4.0(-53,-34,10)/3.9(45,-34,13)
	Transverse Temporal Gyrus	41, 42	0.4/0.8	2.6(-50,-26,10)/3.7(45,-31,13)
	Lingual Gyrus	18, 17, 19	2.9/2.5	3.0(-21,-87,-1)/3.5(18,-88,-3)
	Lateral Ventricle		0.5/1.2	2.6(-36,-35,-6)/3.2(36,-32,-8)
	Cerebellum		4.6/0.7	3.2(-18,-57,-35)/2.5(21,-56,-10)
	Basal Ganglia		1.6/0.7	3.0(-24,-15,-2)/2.9(30,-18,-4)
	Thalamus		0.1/1.0	1.9(-15,-15,1)/2.9(15,-17,17)
	Insula	13, 45	2.3/2.1	2.7(-30,1,17)/2.8(50,-22,20)
	Superior Occipital Gyrus	18, 19	0.6/0.1	2.7(-30,-82,-3)/2.0(21,-88,-8)
	Supramarginal Gyrus	40	0.5/0.2	2.2(-39,-42,33)/2.6(45,-36,35)
	Anterior Cingulate	10, 33, 32, 24	1.8/0.7	2.5(-12,29,-6)/2.5(12,13,24)
	Middle Occipital Gyrus	18	0.4/0.1	2.5(-27,-84,2)/1.8(36,-76,1)
	Inferior Frontal Gyrus	47, 13, 9, 45, 6	1.2/0.4	2.5(-21,32,-7)/1.8(48,1,19)
	Cuneus	17, 18	0.6/0.2	2.3(-6,-84,7)/2.1(15,-93,0)
	Precuneus	31, 23, 7	0.8/NA	2.1(-12,-63,28)/NA
	Inferior Temporal Gyrus	21, 37	0.2/NA	1.9(-56,-12,-15)/NA
	Posterior Cingulate	31	0.1/NA	1.7(-3,-60,22)/NA

Table 2: Talairach table for auditory oddball

	<i>Area</i>	<i>Brodmann Area</i>	<i>L/R Volume</i>	<i>L/R random effects, Max T (x, y, z)</i>	
<i>Magnitude</i>	Superior Temporal Gyrus	22, 21, 41, 38, 42, 13, 39	27.9/21.7	10.7(-59,-20,1)/8.2(59,-29,10)	
	Middle Frontal Gyrus	46, 6, 9, 8, 10	18.8/5.8	6.9(-45,16,27)/5.4(39,16,27)	
	Inferior Frontal Gyrus	9, 45, 46, 47, 13, 44, 10	17.3/6.8	7.2(-45,24,13)/5.5(39,20,-1)	
	Middle Temporal Gyrus	21, 22, 38, 39	14.8/6.8	9.8(-48,-21,-4)/7.2(50,-18,-4)	
	Insula	13, 22, 47, 41, 40, 45	6.2/8.1	7.3(-42,-23,1)/7.3(45,-15,-2)	
	Superior Frontal Gyrus	6, 8, 10, 9	6.0/1.0	5.3(-6,14,49)/4.6(3,17,49)	
	Lingual Gyrus	17, 18	4.4/1.7	5.6(-18,-93,-3)/4.7(3,-87,-1)	
	Thalamus		3.2/1.1	4.6(-12,-9,3)/4.3(6,-9,0)	
	Inferior Parietal Lobule	40	2.5/1.9	4.9(-62,-37,24)/4.3(45,-34,24)	
	Cuneus	17, 18	2.3/1.3	5.8(-15,-93,0)/4.4(3,-93,0)	
	Medial Frontal Gyrus	8, 6, 32	2.2/0.9	5.4(-6,20,46)/4.4(3,17,46)	
	Transverse Temporal Gyrus	41, 42	1.6/1.8	6.6(-50,-26,10)/7.5(45,-31,13)	
	Caudate		1.4/1.5	5.6(-12,1,19)/5.0(9,4,16)	
	Postcentral Gyrus	40, 43	1.4/1.7	6.1(-65,-23,15)/6.6(56,-25,15)	
	Cingulate Gyrus	32, 23	1.3/0.8	4.2(-12,-2,28)/4.1(3,-22,26)	
	Precentral Gyrus	44, 6, 9, 13	1.3/0.6	5.0(-53,5,44)/5.3(45,18,7)	
	Cerebellum		0.5/6.2	3.8(0,-74,-14)/5.4(15,-80,-24)	
	Parahippocampal Gyrus		0.5/0.6	4.5(-33,-4,-17)/4.6(27,-9,-12)	
	Supramarginal Gyrus	40	0.5/NA	3.8(-62,-46,22)/NA	
	Inferior Occipital Gyrus	17	0.1/NA	3.1(-21,-97,-8)/NA	
	Inferior Temporal Gyrus	21	0.1/NA	3.6(-56,-7,-15)/NA	
	Posterior Cingulate	23	NA/0.1	NA/3.5(3,-28,24)	
	<i>Positive Phase</i>	Superior Temporal Gyrus	22	NA/0.7	NA/3.7(36,-1,-15)
		Insula	13	NA/1.0	NA/3.5(39,-17,4)
		Parahippocampal Gyrus		NA/0.2	NA/3.3(33,-4,-15)
		Middle Temporal Gyrus	21	NA/0.1	NA/2.3(42,4,-28)
	<i>Negative Phase</i>	Inferior Parietal Lobule	40	3.7/0.7	3.6(-53,-42,24)/5.8(48,-46,22)
Middle Temporal Gyrus		21, 39, 22, 37	1.2/1.4	4.4(-48,-41,2)/4.7(53,-46,8)	
Insula		13, 47	2.5/0.4	4.3(-45,-40,19)/3.4(39,21,13)	
Supramarginal Gyrus		40	1.8/0.2	4.3(-50,-45,30)/4.1(50,-48,22)	
Inferior Frontal Gyrus		45, 6, 9, 47, 13, 46	2.6/1.9	4.0(-39,2,30)/4.0(42,21,13)	
Cingulate Gyrus		24	2.2/0.2	3.8(-9,-7,39)/2.5(3,-13,37)	
Precentral Gyrus		6, 9	1.1/NA	3.6(-42,1,28)/NA	
Caudate			0.2/NA	3.3(-12,-2,17)/NA	
Postcentral Gyrus		40	0.6/NA	3.1(-53,-23,15)/NA	
Middle Frontal Gyrus		9, 11, 46, 47	0.2/0.5	2.2(-48,5,36)/3.0(36,41,-5)	
Superior Frontal Gyrus		6	NA/0.5	NA/3.0(9,6,63)	
Inferior Temporal Gyrus		37, 21	NA/0.1	NA/2.7(65,-53,-5)	
Medial Frontal Gyrus		6	0.6/0.2	2.6(-12,3,58)/2.6(3,3,52)	
Angular Gyrus			0.1/NA	2.3(-36,-54,30)/NA	

The color activation maps in Figure 4.7 show the correspondence between the magnitude and phase response. The regions of interest in each of these maps are labeled such that red shows magnitude only areas, green shows phase only, and the areas for magnitude and phase are shown by blue. Tables 3 and 4 give us the corresponding peak activations and their talairach coordinates for motor tapping and auditory oddball tasks. Tapping movement mainly activates regions in the motor cortex, hence for the motor tapping paradigm it is expected to see peaks in precentral

gyrus. All the sub-sections in Table 3 show activation/peaks in this area. From the auditory oddball paradigm, it is a known fact that the novels mainly activate the temporal lobes; Table 4 shows peak activations in the superior temporal gyrus in all the sub-sessions.

Table 3: Talairach table for RGB maps of motor tapping

<i>Mag (Mag & Phs)</i>	<i>Area</i>	<i>Brodman Area</i>	<i>L/R Volume</i>	<i>L/R random effects, Max T (x, y, z)</i>
	Precentral Gyrus	4, 6	0.0/3.3	2.6(-45,-21,37)/14.1(36,-12,56)
	Postcentral Gyrus	3, 2, 40	0.1/3.9	3.1(-48,-21,40)/13.0(36,-21,45)
	Cerebellum		5.1/NA	12.8(-21,-56,-17)/NA
	Middle Frontal Gyrus	6	NA/0.9	NA/10.1(27,-11,61)
	Medial Frontal Gyrus	6	0.4/1.3	5.8(0,-3,50)/7.1(6,-3,53)
	Inferior Parietal Lobule	40	NA/2.8	NA/6.7(45,-30,46)
	Cingulate Gyrus	24, 31	0.5/0.9	5.3(0,-1,47)/6.3(6,-1,47)
	Fusiform Gyrus	37	0.1/NA	6.3(-21,-53,-10)/NA
	Superior Frontal Gyrus	6	NA/0.1	NA/4.3(6,8,49)
	Insula	13	NA/0.2	NA/4.2(50,-22,20)
	Paracentral Lobule		0.0/0.1	2.8(0,-9,47)/3.8(6,-9,47)
	Parahippocampal Gyrus		0.0/NA	3.2(-21,-47,-10)/NA
	Basal Ganglia		NA/0.0	NA/3.2(33,3,-5)
	Thalamus		NA/0.1	NA/3.0(15,-20,15)
	Transverse Temporal Gyrus		NA/0.0	NA/2.8(53,-26,12)
	Superior Temporal Gyrus	41, 22	NA/0.1	NA/2.6(50,-31,15)
<i>Mag(Only Mag)</i>	<i>Area</i>	<i>Brodman Area</i>	<i>L/R Volume</i>	<i>L/R random effects, Max T (x, y, z)</i>
	Precentral Gyrus	4, 6, 44	4.8/17.2	4.4(-56,5,36)/14.9(39,-15,56)
	Postcentral Gyrus	3, 4, 2, 1, 40, 5, 43, 7	3.5/12.0	3.3(-50,-21,37)/13.9(42,-18,53)
	Cerebellum		24.1/12.9	13.8(-21,-53,-18)/7.3(24,-56,-20)
	Middle Frontal Gyrus	6, 9, 8	2.7/5.5	4.4(-56,2,39)/11.6(30,-9,61)
	Superior Frontal Gyrus	6	2.8/3.6	5.7(0,6,52)/11.5(33,-8,64)
	Medial Frontal Gyrus	6, 32	2.8/3.3	6.4(0,3,52)/7.4(6,0,53)
	Fusiform Gyrus	19, 37	0.8/NA	6.7(-21,-56,-10)/NA
	Inferior Parietal Lobule	40	0.6/2.8	3.1(-36,-30,40)/6.6(48,-32,57)
	Cingulate Gyrus	24, 32	0.7/1.7	5.3(0,2,47)/6.2(6,2,47)
	Thalamus		NA/4.9	NA/5.8(15,-17,4)
	Inferior Frontal Gyrus	9, 44, 45, 47	2.1/2.3	4.3(-56,7,33)/5.5(59,7,27)
	Lingual Gyrus	18, 19	1.2/0.1	5.0(-18,-70,-9)/2.7(3,-76,-6)
	Basal Ganglia		0.7/5.8	2.8(-21,-3,-2)/4.9(21,-6,-5)
	Insula	13, 40	0.5/5.2	2.9(-45,9,-3)/4.8(48,3,3)
	Superior Temporal Gyrus	22, 41, 38, 42	1.5/4.0	3.1(-48,9,-3)/4.6(50,3,0)
	Superior Parietal Lobule	7, 5	NA/1.2	NA/3.8(30,-47,60)
	Precuneus	7	NA/0.1	NA/3.3(30,-47,52)
	Transverse Temporal Gyrus	41, 42	NA/0.6	NA/3.0(56,-17,12)
	Parahippocampal Gyrus		NA/0.2	NA/3.0(27,-4,-12)
<i>Neg Phs(Mag & Phs)</i>	<i>Area</i>	<i>Brodman Area</i>	<i>L/R Volume</i>	<i>L/R random effects, Max T (x, y, z)</i>
	Postcentral Gyrus	3, 2, 40	NA/3.9	NA/7.9(33,-24,43)
	Cingulate Gyrus	24, 31	0.5/0.9	6.9(0,-7,45)/7.3(3,-7,45)
	Paracentral Lobule		0.0/0.1	6.5(0,-9,47)/7.1(3,-9,47)
	Medial Frontal Gyrus	6	0.3/1.3	5.8(0,-9,50)/6.6(3,-9,50)
	Precentral Gyrus	4	0.1/1.5	3.3(-36,-13,39)/6.2(39,-21,37)
	Cerebellum		2.6/NA	5.8(-27,-44,-15)/NA
	Parahippocampal Gyrus		0.0/NA	5.5(-21,-47,-10)/NA
	Inferior Parietal Lobule	40	NA/2.8	NA/5.5(45,-25,29)
	Fusiform Gyrus	37	0.1/NA	4.3(-21,-53,-7)/NA
	Middle Frontal Gyrus	6	NA/0.1	NA/4.0(24,-7,45)
	Superior Temporal Gyrus	41	NA/0.1	NA/3.0(48,-31,15)
	Insula	13	NA/0.1	NA/2.8(50,-22,20)
	Thalamus		NA/0.1	NA/2.6(15,-20,15)
	Basal Ganglia		NA/0.0	NA/2.6(27,-18,-2)
	Transverse Temporal Gyrus		NA/0.0	NA/2.6(53,-26,12)
<i>Pos Phs(Mag & Phs)</i>	<i>Area</i>	<i>Brodman Area</i>	<i>L/R Volume</i>	<i>L/R random effects, Max T (x, y, z)</i>
	Precentral Gyrus	6	0.0/1.8	2.6(-45,-21,37)/4.8(36,-12,45)
	Middle Frontal Gyrus	6	NA/0.8	NA/4.7(33,-12,45)
	Cerebellum		2.5/NA	4.7(-18,-62,-15)/NA

	Postcentral Gyrus	2, 3	0.1/NA	2.9(-48,-21,43)/NA
	Medial Frontal Gyrus	6	0.0/0.1	2.5(-15,8,52)/2.8(9,8,52)
	Superior Frontal Gyrus	6	NA/0.1	NA/2.8(6,8,52)
	Insula		NA/0.1	NA/2.7(45,6,-3)
	Superior Temporal Gyrus	22	NA/0.1	NA/2.7(53,-11,9)
	Basal Ganglia		NA/0.0	NA/2.6(33,3,-5)
<i>Neg Phs(Only Phs)</i>	Area	Brodman Area	L/R Volume	L/R random effects, Max T (x, y, z)
	Paracentral Lobule	31, 6	0.2/0.8	6.3(0,-9,45)/6.6(3,-9,45)
	Cingulate Gyrus	24, 31	2.3/3.3	5.7(-3,-7,45)/6.2(3,-7,42)
	Medial Frontal Gyrus	6	0.4/1.7	5.3(0,-12,48)/5.0(6,-15,48)
	Cerebellum		1.1/0.2	5.2(-30,-44,-15)/2.8(24,-42,-21)
	Parahippocampal Gyrus	37, 19, 36	0.7/0.4	4.8(-24,-47,-10)/3.7(36,-33,-11)
	Inferior Parietal Lobule	40	NA/1.6	NA/4.5(36,-25,29)
	Precentral Gyrus	6, 4	1.7/NA	4.3(-36,-10,42)/NA
	Fusiform Gyrus	37, 19, 20	0.6/0.3	4.2(-24,-50,-8)/3.6(36,-36,-11)
	Middle Temporal Gyrus	22, 21	3.8/0.1	4.0(-56,-35,-1)/2.6(48,-32,2)
	Middle Frontal Gyrus	6	0.4/NA	4.0(-30,-12,45)/NA
	Superior Temporal Gyrus	41, 22, 42, 21	2.3/3.4	4.0(-53,-34,10)/3.9(45,-34,13)
	Postcentral Gyrus	2	NA/0.1	NA/3.8(50,-30,35)
	Transverse Temporal Gyrus	41	0.0/0.2	2.6(-50,-26,10)/3.7(45,-31,13)
	Lingual Gyrus	18	0.5/0.6	3.0(-21,-87,-1)/3.5(18,-88,-3)
	Basal Ganglia		0.3/0.2	3.0(-24,-15,-2)/2.9(30,-18,-4)
	Thalamus		NA/0.0	NA/2.9(15,-17,17)
	Insula		0.1/NA	2.7(-30,1,17)/NA
	Inferior Occipital Gyrus	18	0.1/NA	2.7(-30,-82,-3)/NA
	Supramarginal Gyrus		NA/0.1	NA/2.6(45,-36,35)
	Anterior Cingulate		0.1/NA	2.5(-12,29,-6)/NA
<i>Pos Phs(Only Phase)</i>	Area	Brodman Area	L/R Volume	L/R random effects, Max T (x, y, z)
	Precentral Gyrus	43, 6, 13, 9	1.3/0.1	4.0(-39,-19,34)/2.8(39,-10,39)
	Postcentral Gyrus	3, 2	1.0/NA	3.7(-39,-16,31)/NA
	Middle Frontal Gyrus	6	0.2/1.3	2.8(-33,6,52)/3.6(27,6,55)
	Precuneus	7, 31	0.6/0.2	3.2(-15,-50,49)/2.7(3,-59,44)
	Cingulate Gyrus	31	0.2/0.1	3.2(-15,-42,27)/2.8(12,-42,27)
	Superior Temporal Gyrus	22	0.1/0.0	2.6(-50,-3,3)/2.9(50,-11,9)
	Posterior Cingulate		NA/0.0	NA/2.8(12,-42,24)
	Medial Frontal Gyrus		NA/0.2	NA/2.8(21,5,49)
	Insula		0.1/0.0	2.6(-45,-11,17)/2.5(36,-8,11)
	Middle Temporal Gyrus		0.0/NA	2.5(-42,-61,3)/NA
	Paracentral Lobule	5	NA/0.0	NA/2.5(18,-41,55)
	Superior Frontal Gyrus		NA/0.0	NA/2.5(30,11,49)

Table 4: Talairach table for RGB maps of auditory oddball

<i>Mag (Mag & Phs)</i>	<i>Area</i>	<i>Brodman Area</i>	<i>L/R Volume</i>	<i>L/R random effects, Max T (x, y, z)</i>
	Superior Temporal Gyrus	21, 22, 42, 41, 13, 38, 39	5.5/4.0	8.9(-56,-12,-2)/8.2(59,-29,10)
	Insula	13, 47	1.0/1.0	5.8(-56,-37,18)/7.3(45,-15,-2)
	Inferior Frontal Gyrus	45, 47, 13, 9	2.2/0.9	7.2(-45,24,13)/5.5(45,18,10)
	Middle Temporal Gyrus	21, 22, 39	1.0/0.8	7.0(-50,-38,5)/4.3(53,-43,8)
	Transverse Temporal Gyrus	41	0.0/NA	5.3(-53,-23,12)/NA
	Caudate		0.2/NA	5.2(-12,-2,19)/NA
	Middle Frontal Gyrus	9	0.2/0.0	5.1(-45,8,38)/3.7(42,22,24)
	Inferior Parietal Lobule	40	0.7/0.1	4.9(-62,-37,24)/3.7(53,-40,24)
	Postcentral Gyrus	40	0.2/NA	4.9(-56,-25,15)/NA
	Precentral Gyrus	6, 9	0.3/NA	4.3(-50,-8,6)/NA
	Supramarginal Gyrus	40	0.3/0.0	3.5(-53,-36,32)/3.1(56,-46,22)
	Parahippocampal Gyrus		NA/0.1	NA/3.5(33,-9,-15)
	Cingulate Gyrus		0.1/NA	3.3(-12,-4,28)/NA
	Superior Frontal Gyrus	6	NA/0.0	NA/3.0(3,6,52)
<i>Mag(Only Mag)</i>	Area	Brodman Area	L/R Volume	L/R random effects, Max T (x, y, z)
	Superior Temporal Gyrus	22,21,41,38,42,13,39	21.4/18.8	10.7(-59,-20,1)/8.2(56,-29,10)
	Middle Temporal Gyrus	21,22,38,39	12.5/5.7	9.8(-48,-21,-4)/7.2(50,-18,-4)
	Transverse Temporal Gyrus	41,42	1.5/1.8	5.8(-45,-29,10)/7.5(45,-31,13)
	Insula	13,22,47,41,40,45	4.2/7.3	6.9(-42,-20,1)/7.3(45,-15,-2)
	Inferior Frontal Gyrus	9,45,46,47,13,44,10	14.9/5.6	7.0(-48,24,13)/5.5(39,20,-1)
	Middle Frontal Gyrus	46,6,9,8,10	18.6/5.8	6.9(-45,16,27)/5.4(39,16,27)

Postcentral Gyrus	40,43	1.0/1.7	6.1(-65,-23,15)/6.6(56,-25,15)	
Cuneus	17,18	2.3/1.3	5.8(-15,-93,0)/4.4(3,-93,0)	
Lingual Gyrus	17,18	3.2/1.6	5.6(-18,-93,-3)/4.7(3,-87,-1)	
Cerebellum		0.1/6.1	5.0(-53,5,44)/5.4(15,-80,-24)	
Medial Frontal Gyrus	8,6,32	2.2/0.9	5.4(-6,20,46)/4.4(3,17,46)	
Precentral Gyrus	44,6,9,13	1.1/0.6	5.0(-53,5,44)/5.3(45,18,7)	
Superior Frontal Gyrus	6,8,10,9	6.0/1.0	5.3(-6,14,49)/4.6(3,17,49)	
Caudate		0.4/1.2	4.9(-9,4,16)/5.0(9,4,16)	
Inferior Parietal Lobule	40	2.1/1.7	4.9(-62,-37,24)/4.3(45,-34,24)	
Parahippocampal Gyrus		0.5/0.6	4.5(-33,-4,-17)/4.6(27,-9,-12)	
Thalamus		3.2/1.1	4.6(-12,-9,3)/4.3(6,-9,0)	
Basal Ganglia		1.4/0.3	4.5(-12,6,-5)/ 4.4(36,-20,4)	
Cingulate Gyrus	32,23	1.3/0.8	4.2(-12,-2,28)/4.1(3,-22,26)	
Supramarginal Gyrus	40	0.3/NA	3.8(-62,-46,22)/NA	
Inferior Temporal Gyrus	21	0.1/NA	3.6(-56,-7,-15)/NA	
Posterior Cingulate	23	NA/0.1	NA/3.5(3,-28,24)	
Anterior Cingulate	33	NA/0.0	NA/3.4(6,10,22)	
Uncus	28	0.1/0.1	3.1(-30,-1,-20)/3.2(30,5,-20)	
Inferior Occipital Gyrus	17	0.1/NA	3.1(-21,-97,-8)/NA	
<hr/>				
<i>Neg Phs(Mag & Phs)</i>	Area	Brodman Area	L/R Volume	L/R random effects, Max T (x, y, z)
	Superior Temporal Gyrus	22, 13, 39, 41, 42, 21, 38	5.5/3.3	5.7(-48,-40,13)/8.0(50,-46,13)
	Middle Temporal Gyrus	21, 39, 22	1.0/0.8	4.4(-48,-41,2)/4.7(53,-46,8)
	Insula	13, 47	1.0/0.3	4.3(-45,-40,19)/3.4(39,21,13)
	Inferior Frontal Gyrus	45, 47, 13, 9	2.2/0.9	4.0(-39,2,30)/4.0(42,21,13)
	Precentral Gyrus	6, 9	0.3/NA	3.6(-39,1,28)/NA
	Inferior Parietal Lobule	40	0.7/0.1	3.5(-56,-37,24)/3.3(50,-40,24)
	Caudate		0.2/NA	3.3(-12,-2,17)/NA
	Postcentral Gyrus	40	0.2/NA	3.1(-53,-23,15)/NA
	Cingulate Gyrus		0.1/NA	2.9(-15,-4,28)/NA
	Transverse Temporal Gyrus	41	0.0/NA	2.7(-53,-23,12)/NA
	Supramarginal Gyrus	40	0.3/0.0	2.5(-50,-39,35)/2.2(56,-46,22)
	Superior Frontal Gyrus	6	NA/0.0	NA/2.3(3,6,52)
	Middle Frontal Gyrus	9	0.2/0.0	2.2(-48,5,36)/2.1(42,22,24)
<hr/>				
<i>Pos Phs(Mag & Phs)</i>	Area	Brodman Area	L/R Volume	L/R random effects, Max T (x, y, z)
	Superior Temporal Gyrus	22	NA/0.7	NA/3.7(36,-1,-15)
	Insula	13	NA/0.7	NA/3.5(39,-17,4)
	Parahippocampal Gyrus		NA/0.1	NA/3.3(33,-4,-15)
<hr/>				
<i>Neg Phs(Only Phs)</i>	Area	Brodman Area	L/R Volume	L/R random effects, Max T (x, y, z)
	Superior Temporal Gyrus	13, 39	0.4/0.6	4.0(-39,-40,10)/6.5(48,-46,19)
	Inferior Parietal Lobule	40	0.9/0.6	3.6(-53,-42,24)/5.8(48,-46,22)
	Supramarginal Gyrus	40	1.1/0.2	4.3(-50,-45,30)/4.1(50,-48,22)
	Inferior Frontal Gyrus	6, 9, 46	0.3/0.8	3.8(-39,-1,30)/3.5(36,29,7)
	Precentral Gyrus	6	0.4/NA	3.6(-42,1,28)/NA
	Insula	13	0.7/NA	3.3(-42,-40,19)/NA
	Middle Temporal Gyrus	37, 21, 39	0.2/0.4	3.3(-39,-43,8)/3.3(65,-53,-2)
	Middle Frontal Gyrus	11, 46, 47	NA/0.3	NA/3.0(36,41,-5)
	Inferior Temporal Gyrus	37	NA/0.0	NA/2.7(65,-53,-5)
	Cingulate Gyrus		0.0/NA	2.7(-15,-4,31)/NA
	Postcentral Gyrus		0.1/NA	2.5(-53,-22,18)/NA
	Basal Ganglia		0.1/NA	2.5(-30,12,-1)/NA
<hr/>				
<i>Pos Phs(Only Phase)</i>	Area	Brodman Area	L/R Volume	L/R random effects, Max T (x, y, z)
	Parahippocampal Gyrus		NA/0.1	NA/3.2(33,-7,-17)
	Insula		NA/0.2	NA/2.9(39,-14,6)
	Basal Ganglia		NA/0.1	NA/2.8(36,-17,4)
	Superior Temporal Gyrus		NA/0.1	NA/2.3(45,5,-20)
	Middle Temporal Gyrus	21	NA/0.1	NA/2.3(42,4,-28)

The results are encouraging and corroborate with patterns observed in the ROI analysis.

The presence of these areas in phase only activation maps (without any magnitude activation)

gives us enough evidence to suggest that using the phase data in fMRI may provide important information.

CHAPTER 5

CONCLUSIONS AND FUTURE WORKS

We have evaluated the correspondence between task-related changes in magnitude and phase data with the expectation that the changes also occur in phase. The goal was to verify whether the phase changes were observed in both block and event-related design studies and if so, to determine if these changes were in regions expected to be involved in the tasks. The secondary goal was to see if any special preprocessing steps for phase were necessary. Different processing strategies like phase motion correction, band-pass filtering, Gaussian smoothing, complex de-noising by discrete wavelet transforms have been implemented and the effects were analysed. It was observed that ICA performs a better job on temporal filtered (band-pass filtering) fMRI data. The activations were studied using different processing methods including region of interest analysis (ROI) and whole brain analysis. Results illustrate that the activations in phase were consistent with the activations in magnitude in both the experimental paradigms. The ROI analysis of motor tapping (MT) data and auditory odd ball (AOD) showed both positive and negative phase activations. Both ROI analysis and the whole brain analysis show phase activation in the expected regions where the magnitude activations are insignificant suggesting that the phase data might hold useful information.

The results show observable phase changes at group level, which suggests that the information in the phase can increase the ability to isolate the task-related functional changes. To our knowledge this is the first attempt to study the phase changes in fMRI BOLD experiments for an event-related design at a group level. However, further research is required to develop

flexible methods to analyze the complex-valued fMRI with the goal to improve the detection efficiency of the task-related changes. Some of this work has been submitted in peer-reviewed journal for publication and is under review. Based on the results we can conclude that both block-design and event-related tasks indicate the presence of task related information in the phase data evaluated at a group level.

REFERENCES

- Ashburner, J. and K. J. Friston (2003). Rigid body registration. Human brain function. R.S.J.Frackowiak, K. J. Friston, C. Frith et al. San Diego, Academic Press.
- Bandettini, P. A., A. Jesmanowicz et al. (1993). "Processing strategies for time-course data sets in functional mri of the human brain." *Magnetic Resonance In Medicine* 30(2): 161-173.
- Brammer, M. J. (2001). Head motion and its correction. *Functional MRI: An introduction to methods*. P. Jezzard, P. M. Matthews and S. M. Smith. New York, Oxford University Press Inc: 243-250.
- Calhoun, V. D., T. Adali et al. (2002). "Independent component analysis of fMRI data in the complex domain." *Magnetic Resonance In Medicine* 48(1): 180-192.
- Deshmukh, A. V., V. Shivhare et al. (20-22 Dec. 2004). A phase based method for investigating the functional connectivity in the fMRI data. India Annual Conference, 2004. Proceedings of the IEEE INDICON 2004.
- Detre, J. A. and J. Wang (2002). "Technical aspects and utility of fMRI using BOLD and ASL." *Clinical Neurophysiology*(133): 621-634.
- Feng, Z., A. Caprihan et al. (2009). "Biophysical Modeling of Phase Changes in BOLD fMRI." *NeuroImage* 47: 540-548.
- Filzmoser P, Baumgartner R et al. (1999). "A hierarchical clustering method for analyzing functional MR images." *Magn Reson Imaging*(17): 817-826.
- Freire, L. and J. F. Mangin (2001). "Motion Correction Algorithms May Create Spurious Brain Activations in the Absence of Subject Motion." *NeuroImage* 14(3): 709-722.
- Freire, L., A. Roche et al. (2002). "What is the best similarity measure for motion correction in fMRI time series?" *Medical Imaging, IEEE Transactions on* 21(5): 470-484.
- Friston, K. J., C. Frith et al. (1995). "Characterizing dynamic brain responses with fMRI." *NeuroImage*(2): 166-172.
- Heeger, D. J. and D. Ress (2002). "What does fMRI tell us about neuronal activity?" *Nature Reviews Neuroscience*(3): 142-151.
- Hoogenraad, F. G. C., P. J. W. Pouwels et al. (2001). "Quantitative differentiation between BOLD models in fMRI." *Magnetic Resonance In Medicine* 45(2): 233-246.
- Hoogenraad, F. G. C., J. R. Reichenbach et al. (1998). "In vivo measurement of changes in venous blood-oxygenation with high resolution functional MRI at 0.95 Tesla by measuring changes in susceptibility and velocity." *Magnetic Resonance In Medicine* 39(1): 97-107.

Hoult, D. I., C. N. Chen et al. (1984). "Quadrature Detection in the Laboratory Frame." *Magn Reson Med*(1): 339-353.

Laird, A. R., B. P. Rogers et al. (2002). "Characterizing instantaneous phase relationships in whole-brain fMRI activation data." *Human Brain Mapping* 16(2): 71-80.

Lee, J., M. Shahram et al. (2007). "Complex data analysis in high-resolution SSFP fMRI." *Magnetic Resonance In Medicine* 57(5): 905-917.

Lynn, P. A. (1989). *Introduction to the Analysis and Processing of Signals*, Hemisphere Publishing Corporation.

Menon, R. S. (2002). "Postacquisition suppression of large-vessel BOLD signals in high-resolution fMRI." *Magnetic Resonance In Medicine* 47(1): 1-9.

Miller, K. L., B. A. Hargreaves et al. (1-5 Sept. 2004). Functional brain imaging with BOSS FMRI. *Engineering in Medicine and Biology Society, 2004. IEMBS '04. 26th Annual International Conference of the IEEE*. 2: 5234-5237.

Natalia Petridou, Andreas Schäfer et al. (2009). "Phase vs. magnitude information in functional magnetic resonance imaging time series: toward understanding the noise." *Magnetic Resonance Imaging*(In Press).

Ogawa, S., T. M. Lee et al. (1990). "Oxygenation-sensitive contrast in magnetic resonance imaging of rodent brain at high magnetic fields." *Magnetic Resonance in Medicine*(14): 68-78.

Pauling, L. and C. D. Coryell (1936). "The magnetic properties and structure of hemoglobin, oxyhemoglobin and carbomonoxihemoglobin." *Proceedings of the National Academy of Sciences, USA* 22: 210-216.

Rowe, D. B. (2005). "Modeling both the magnitude and phase of complex-valued fMRI data." *NeuroImage* 25(4): 1310-1324.

Rowe, D. B. (2005). "Parameter estimation in the magnitude-only and complex-valued fMRI data models." *NeuroImage* 25(4): 1124-1132.

Rowe, D. B. and R. B. Logan (2004). "A complex way to compute fMRI activation." *NeuroImage* 23(3): 1078-1092.

Rowe, D. B. and R. B. Logan (2005). "Complex fMRI analysis with unrestricted phase is equivalent to a magnitude-only model." *NeuroImage* 24(2): 603-606.

Smith, S. M. (2001). Preparing fMRI data for statistical analysis. *Functional MRI: An introduction to methods*. P. Jefferies, P. M. Matthews and S. M. Smith. New York, Oxford University Press Inc: 229-241.

Tomasi, D. G. and E. C. Caparelli (2007). "Macrovascular contribution in activation patterns of working memory." *Epub* 27(1): 33-42.

Weaver, J. B. (1999). "Applications of monotonic noise reduction algorithms in fMRI, phase estimation, and contrast enhancement." *International Journal of Imaging Systems and Technology* 10(2): 177-185.

Zaroubi, S. and G. Goelman (2000). "Complex denoising of MR data via wavelet analysis: Application for functional MRI." *Magn Reson Imaging*(18): 59-68.

Zhao, F., T. Jin et al. (2007). "Sources of phase changes in BOLD and CBV-weighted fMRI." *Magn Reson Med* 57(3): 520-527.